Geological Society, London, Special Publications Online First

Oxidation processes and their effects on the magnetic remanence of Early Cretaceous subaerial basalts from Sierra Chica de Córdoba, Argentina

S. E. Geuna, S. L. Lagorio and H. Vizán

Geological Society, London, Special Publications, first published September 3, 2014; doi 10.1144/SP396.13

Notes

Oxidation processes and their effects on the magnetic remanence of Early Cretaceous subaerial basalts from Sierra Chica de Córdoba, Argentina

S. E. GEUNA[1]*, S. L. LAGORIO[2] & H. VIZÁN[1]

[1]*IGEBA (CONICET-UBA), Departamento de Cs. Geológicas, Facultad de Ciencias Exactas y Naturales, Universidad de Buenos Aires, Ciudad Universitaria, Pab. 2, C1428EHA Buenos Aires, Argentina*

[2]*IGRM, Servicio Geológico Minero Argentino, Colectora Av. Gral. Paz 5445, edificio 25, Villa Martelli, Buenos Aires, Argentina*

**Corresponding author (e-mail: geuna@gl.fcen.uba.ar)*

Abstract: We carried out magnetic analyses on a sequence of Cretaceous alkaline–transitional subaerial basalts of Córdoba Province, Argentina, which have high-Ti magnetite as the main opaque phase. Three different groups are identified based on the degree of high-temperature oxidation during the lava extrusion, combined with superimposed maghemitization and hematization. In the first group, titanomagnetites are optically homogeneous or exhibit coarse intergrowths with ilmenite. The magnetic susceptibility and its variation with temperature and magnetic field point to Ti-poorer compositions than those indicated by electron microprobe, which is interpreted as due to low-temperature oxidation with subsolvus microexsolution. The second group of basalts suffered moderate high-temperature oxidation, with crowded exsolved ilmenite laths within a Ti-poor magnetite$_{ss}$ host, followed by maghemitization and hematite replacement. The third group shows a strongly advanced degree of low-temperature alteration, with the virtual disappearance of magnetite. Based on magnetic properties and field tests applied to the magnetic remanence, we interpret that maghemitization and hematization must have been responsible for the acquisition of a stable magnetic remanence, in the presence of hydrothermal fluids coeval with volcanism. The most advanced degree of alteration, typical of highly porous amygdaloidal lava flows and volcanic breccias, occurred later, probably due to weathering.

Apparent polar wander paths are important tools for tectonic and geodynamic reconstructions. They are constructed from palaeomagnetic poles selected according to a list of reliability criteria designed to evaluate their quality (see Van der Voo 1993). The poles are calculated from palaeomagnetic directions recorded by both igneous and sedimentary rocks. Among them, igneous rocks have usually been considered as more reliable recorders of the palaeomagnetic field, and some authors only consider palaeomagnetic poles obtained from igneous rocks to calculate apparent polar wander paths (e.g. see Prévot *et al.* 2000). This is because igneous, and particularly extrusive rocks, provide the possibility of obtaining a chronological age for the time of remanence acquisition (coincident with the time of extrusion) through radiometric dating. Moreover, igneous rocks usually carry an instantaneous and unbiased record of the Earth's magnetic field. By contrast, sedimentary lithologies may have long and complex histories of remanence acquisition. Other complications may be due to secondary depositional and physical processes that produce a flattening of palaeomagnetic inclinations (see Tauxe & Kent 2004).

However, igneous rocks also carry palaeomagnetic records that may reflect complex histories during which different magnetic minerals are created, acquiring different components of magnetization. The bulk chemistry of the magma determines the first-formed mineral assemblage of igneous rocks that can be strongly modified later by several factors, such as the rate of cooling, the composition of gases included in the magma, oxidation processes related to the exposure of lava flows to the atmosphere or to oceanic water, or other geological processes that occur after the burial of lava flows.

For example, in basaltic lavas the original titanomagnetite composition is $Fe_{3-x}Ti_xO_4$ with x lying in the range $0.5 < x < 0.8$, and the hematite–ilmenite is $Fe_{2-y}Ti_yO_3$, with y in the range $0.8 < y < 1$ (O'Reilly 1984). On cooling, the system is usually oxidizing with respect to stoichiometric titanomagnetite, and deuteric oxidation occurs, to varying extents, depending on the time

From: Ort, M. H., Porreca, M. & Geissman, J. W. (eds) 2014. *The Use of Palaeomagnetism and Rock Magnetism to Understand Volcanic Processes*. Geological Society, London, Special Publications, **396**, http://dx.doi.org/10.1144/SP396.13

available and the local oxygen pressure. Post-eruptive burial of lavas by younger flows is accompanied by late crystallizing minerals such as zeolites (Alt 1998; Robinson & Bevins 1998), and further changes in the opaque mineral assemblage may occur in an environment where the rocks are saturated by heated meteoric water. Other alterations of the original opaque mineral compositions after burial of lava flows could be due to hydrothermal processes related to large dyke or sill intrusions with hot magmatic residual fluids (Ade-Hall *et al.* 1971). Consequently, the opaque minerals and their magnetic properties may reflect a variety of processes, with the probability of alteration of the original compositions increasing for older basaltic rocks.

The role of post-eruptive transformations is very important for a palaeomagnetic study because they tend to cause the stabilization of magnetic remanence through the subdivision of magnetic grains (Ade-Hall *et al.* 1965; O'Reilly 1984; Dunlop & Özdemir 1997). It is crucial to the understanding of the timing of those transformations to establish whether the stable remanence was acquired early (and is, therefore, representative of the Earth's magnetic field conditions at the time of extrusion) or during a later hydrothermal event.

Correlations between the oxidation state of the iron–titanium oxides and the magnetic properties of lavas have been attempted since the early studies of Ade-Hall *et al.* (1965), Watkins & Haggerty (1965) and Wilson (1966). Low-temperature oxidation in submarine basalts received particular attention (e.g. Johnson & Hall 1978; Hall 1985; Cui *et al.* 1994) because it is a widespread process that drastically changes the intensity and character of the magnetic remanence recorded by the upper oceanic crust, modifying the shape of magnetic anomalies caused by the ocean floor rocks. However, the magnetic properties of subaerial basalts vary widely, strongly controlled by high-temperature oxidation processes, followed by hydrothermal alteration effects (e.g. Ade-Hall *et al.* 1971; Oliva-Urcia *et al.* 2011). The hydrothermal alteration usually causes a reduction in magnetic remanence due to magnetite replacement (e.g. Beske-Diehl & Li 1993; Oliva-Urcia *et al.* 2011), and, depending on the intensity and timing, it can even destroy the original magnetic remanence and replace it with one acquired by newly formed minerals (e.g. Lanza & Zanella 1993; Van der Voo *et al.* 1993).

Since the foundation of the Laboratory of Palaeomagnetism of the Universidad de Buenos Aires in 1964, several palaeomagnetic studies have been carried out in Argentina on igneous rocks. In Sierra Chica de Córdoba, Valencio (1972), Linares & Valencio (1975), Vilas (1976) and Mendía (1978) worked on Cretaceous basalts of the Sierra de los Cóndores Group using now out-dated methodologies. The palaeomagnetic poles published in these venerable papers are still incorporated into apparent polar wander paths to analyse mantle dynamics (see Torsvik *et al.* 2008, 2012). Geuna & Vizán (1998) revisited Sierra Chica de Córdoba and, employing updated methodologies and working protocols, obtained a new palaeomagnetic pole that replaced the previous ones. At the same time, they proposed that magnetic susceptibility, intensity of natural remanent magnetization and the remanent coercive forces of the basalts are controlled by the degree of oxidation, as suggested by the variation in colour of the samples. They found three magnetic components with different magnetic coercive forces interpreted, respectively, as: a viscous magnetization carried by multidomain (titano)magnetite; a chemical or thermochemical magnetization carried by fine-grained (titano)magnetite (possibly single or pseudosingle-domain) that recorded the characteristic remanent magnetization; and a chemical magnetization acquired by hematite resistant to alternating-field demagnetization. On the basis of field tests, Geuna & Vizán (1998) constrained the relative ages of the different magnetizations but they did not perform an exhaustive investigation to determine the precise nature of the magnetic carriers of the remanence.

The aim of our study is to understand the whole process of remanence acquisition for the Sierra Chica de Córdoba basalts. In this paper, we present new and detailed studies (including optical petrography, electron microprobe analysis and magnetic characterization via several rock magnetic experiments) on different magnetic carriers of the Cretaceous basalts. On the basis of these studies, we interpret the probable origins of the magnetic carriers, and deduce the relationship between the stages of remanence acquisition and particular events of the lava cooling history.

Geological setting and sampling

Sierra Chica de Córdoba represents a Neogene north-trending uplift system of the eastern Sierras Pampeanas in Argentina. Outcrops are mainly Precambrian–Early Palaeozoic crystalline basement and an Early Cretaceous volcano-sedimentary complex, formed under extensional tectonics that led to the opening of the South Atlantic Ocean (Uliana *et al.* 1990). Dextral rifting created isolated depocentres as pull-apart basins in all of the Sierra Chica (Schmidt *et al.* 1995), mainly controlled by the Punilla and La Calera faults (Fig. 1). These structures followed zones of crustal weakness (Kraemer *et al.* 1995), such as the suture between the Córdoba terrane and Río de la Plata craton,

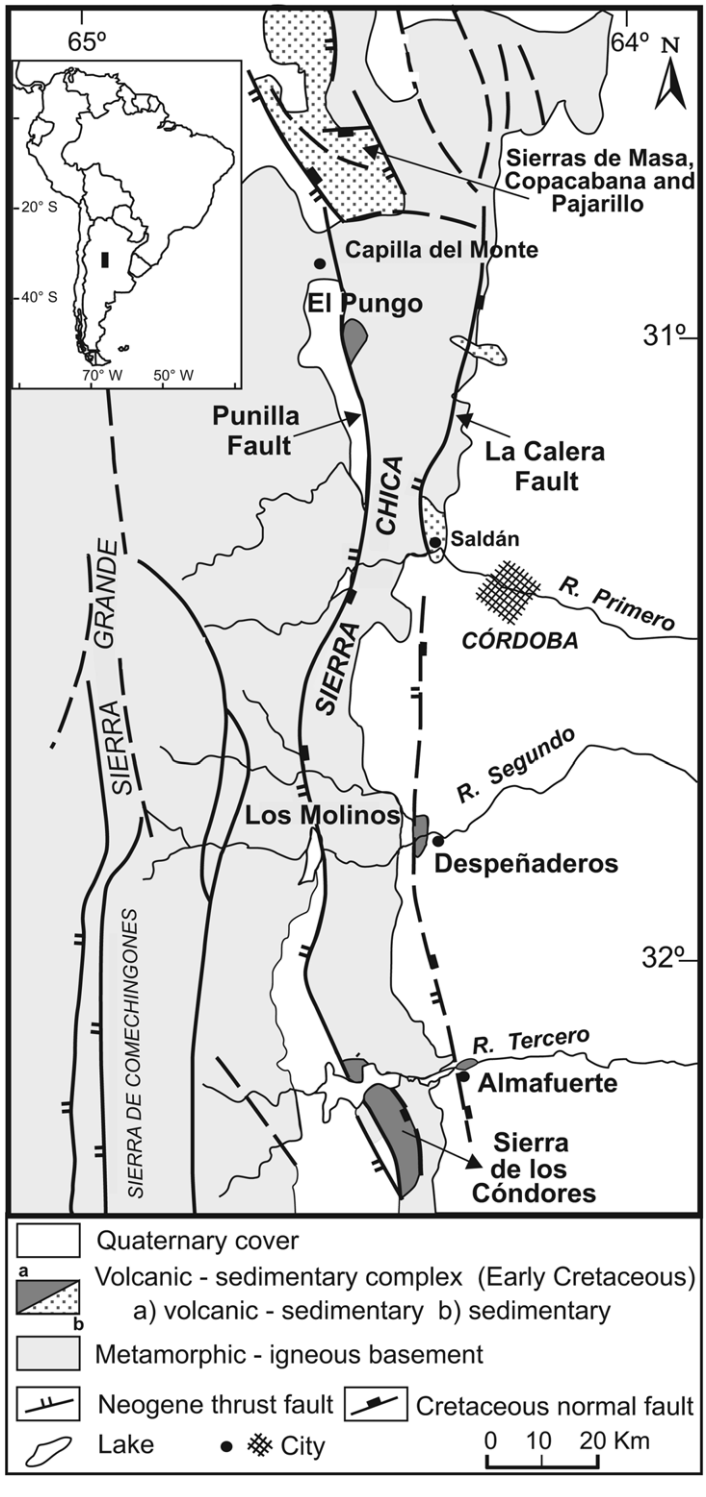

Fig. 1. Geological map of the Sierra Chica de Córdoba, adapted from Gordillo & Lencinas (1980), Schmidt *et al.* (1995) and Kay & Ramos (1996).

represented by the Eastern Córdoba ophiolitic belt (Ramos *et al.* 2000). The uplift of the Sierra Chica by Andean tectonics, within the zone of flat subduction of the Nazca plate, inverted and exposed the Cretaceous complex in the footwall of the normal faults (Schmidt *et al.* 1995).

The Early Cretaceous magmatic outcrops of Sierra Chica represent small remnants of the volcano-sedimentary complex that discordantly rests on the basement. They are composed of red beds with intercalated basic lava flows (Gordillo & Lencinas 1980) assigned to the Sierra de Los Cóndores (Gordillo & Lencinas 1967*a*, 1969, 1980) and El Pungo groups (Gordillo & Lencinas 1967*b*). The volcanic rocks are basic–intermediate and mainly have a potassic alkaline character, defining an alkali-basalt–trachyte suite, a transitional basalt–latibasalt suite and basanites. Details of chemistry and petrology are given by Lagorio (2008).

K–Ar ages on whole rock and sanidines from lava flows and dykes in Sierra de Los Cóndores, Almafuerte and El Pungo range from 133 to 115 Ma (Linares & González 1990). Río Los Molinos dykes are a little older, with an average age of 141 $\pm$ 10 Ma (Linares & Valencio 1975); if younger ages obtained for some of them (average of 67 $\pm$ 5 Ma) then they are excluded on the basis that they were probably reset during Cenozoic times, according to the palaeomagnetic data obtained by Geuna & Vizán (1998).

The Sierra de los Cóndores Group was defined by Gordillo & Lencinas (1967*a*) in the eponymous mountain range (see Fig. 1), where it forms tabular hills no higher than 100 m. The outcrops are not continuous due to soil and vegetation cover but several hills offer good exposures of four–six successive lava flows (up to 15 flows locally), each lying directly on the precedent, or separated by thin sedimentary layers or by brecciated contacts. An interbedded 60–80 m-thick sedimentary sequence composed of coarse fluvial conglomerates appears in a few localities, separating a lower from an upper sequence of lava flows.

The lava flows are usually between 4 and 8 m thick. They are massive, although vesicular structure is common at the base and top of each flow. Vesicles are sometimes filled with calcite and members of the analcime–wairakite series (Lagorio 2008).

Rocks of equivalent chemistry are strikingly different in colour, as already pointed out by Gordillo & Lencinas (1967*a*), who described successions of black and brown trachybasalts alternating in every surveyed profile. The colour variation was related by Gordillo & Lencinas (1967*a*) to prevailing oxidizing conditions during eruption, mainly involving olivine alteration.

In this paper we present the results of studies carried on the samples collected by Geuna &Vizán (1998) and Lagorio (2008), who worked at the same sites studying the Early Cretaceous volcanic event of Sierra Chica de Córdoba. In particular, Geuna & Vizán (1998) studied palaeomagnetic properties of these lava flows, whereas Lagorio (2008) analysed geochemical features. Here we will use the combined sample collection to perform rock magnetic studies that will allow a better interpretation of the nature of the minerals carrying the magnetic remanence. Sampling was distributed across five localities (see Fig. 1): Sierra de los Cóndores (the most extensive), Almafuerte, Despeñaderos, El Pungo and Los Molinos.

In Sierra de los Cóndores, every volcanic unit was sampled along nine sections, obtaining a total of 60 samples. They range in composition from alkaline basalts, trachybasalts and trachyandesites to transitional basalts and latibasalts, with black and brown varieties. Samples were taken from the massive part of each flow, except for three thin, highly amygdaloidal levels.

In addition to lava flows, 10 basaltic clasts of interbedded conglomerate were sampled in three sections of Sierra de los Cóndores. The clasts range in size from about 5 to 20 cm, and vary in colour (brown and black) and structure (massive and vesicular). The magnetic remanence of these and other clasts was used by Geuna & Vizán (1998) to evaluate the timing of remanence acquisition by means of a conglomerate test. We also took two samples from brecciated contacts of lava flows.

Additional samples (one sample from every flow/dyke) were obtained from limited outcrops of Sierra Chica: three lava flows (trachyandesitic and trachybasaltic compositions) and one dyke (alkaline basalt) in Almafuerte, eight lava flows in Despeñaderos (transitional basalts) and five in El Pungo (basanites and alkaline basalts). Three dykes of alkaline basalt and ankaratrites intruding the metamorphic basement in Los Molinos were also sampled.

Methods and laboratory procedures

The 92 samples (representative of 76 lava flows, two volcanic breccias, four dykes and 10 clasts in conglomerates) were submitted to alternating-field demagnetization, acquisition of isothermal remanent magnetization and backfield demagnetization. According to the range of behaviours observed from these methods, we selected 20 representative samples of diverse lithologies in order to carry out mineralogical investigations and further rock magnetic experiments to identify mineral compositions.

Remanent magnetization was measured using either a Schonstedt or a Digico spinner magnetometer. Samples with a low intensity of magnetization

were measured using a 2G DC squid cryogenic magnetometer. Alternating-field demagnetization (AF) was carried out to a maximum of 110 mT (peak) using a three-axis static 2G600 demagnetizer.

Isothermal remanent magnetization (IRM) of up to 2.3 T along the $+z$ axis and backfield along the $-z$ axis were imparted by using an ASC IM-10–30 pulse magnetizer at the Universidad de Buenos Aires, and measured with a Digico spinner magnetometer. IRM acquisition curves were fitted by cumulative log-Gaussian (CLG: Robertson & France 1994) functions using the software developed by Kruiver *et al.* (2001).

Hysteresis loops were measured at room temperature in a maximum field of 1 T, using a Molspin vibrating sample magnetometer at the Instituto Astronomico e Geofisico (IAG), Universidade de Sao Paulo, Brazil. Thermomagnetic curves were determined using a MS2WF furnace added to a MS2W Bartington susceptometer at the IAG, or a CS4/CSL furnace added to a MFK1 Agico Kappabridge at the Universidad de Buenos Aires. The latter was also used to determine magnetic susceptibility in low field (200 A m^{-1}), and the field- and frequency-dependence of susceptibility.

The identification of opaque phases, together with their textural relationships, character and amount of alteration, was performed on polished and thin sections. The sections were examined using both air and oil immersion objectives with an Axiolab Pol (Carl Zeiss) reflected-light microscope at the Departamento de Ciencias Geológicas at the Universidad de Buenos Aires.

Electron microprobe analyses were performed in 13 of the 20 samples, selected as representative of different magnetic behaviours with peculiar geochemical features, as highlighted by Lagorio (2008). The analyses were carried out by a Cameca-Camebax operating at 15 kV and 15 nA at the Dipartimento di Mineralogia e Petrologia of Padova University (Italy). The PAP-Cameca program was used to convert X-ray counts into weight percentage (wt%) of the corresponding oxides. Results are considered accurate within 2–3% for major elements and 9% for minor elements. Analyses of Fe–Ti oxides were recalculated on the basis of oxide stoichiometry to determine Fe_2O_3 and FeO from total Fe.

Results

Polished sections and microprobe analyses

The terminology used hereafter follows that of Buddington & Lindsley (1964). 'Titanomagnetite' or '(Ti)magnetite' will designate any mineral that is predominantly magnetite and in which titanium-bearing compounds are present either in solid solution or as included phases. Following common usage, 'spinel cubic series' and 'rhombohedral series' may be used for convenience in place of 'magnetite–ulvöspinel series' and 'hematite–ilmenite series', respectively. Intermediate compositions of the solid-solution series are given the name of the supposed nearer end member: for example, $ilmenite_{ss}$ refers to an ilmenite-rich ilmenite–$hematite_{ss}$.

In the case of grains showing evidence of oxidation exsolution, the classification system of Haggerty (1976, 1991) was used to describe the extent of oxidation exsolution of magnetite–ulvöspinel C (cubic) and ilmenite R (rhombohedral) solid-solution members.

Titanomagnetite was revealed as the dominant primary opaque mineral in the studied rocks. It mainly appears as anhedral to subhedral equidimensional crystals, in some cases displaying slightly embayed to highly corroded shapes. Many sections show quadrangular, octagonal and triangular shapes typical of cubic symmetry. Phenocrysts and/or microphenocrysts of titanomagnetite are not common; they only appear in the more evolved rocks (e.g. trachyandesites, trachytes, trachyphonolites) that are volumetrically subordinate lithotypes. Therefore, titanomagnetite mainly forms part of the intergranular groundmass of these volcanic rocks, with a crystal mean dimension of 0.025 mm. Small titanomagnetite crystals in feldspar and mafic microminerals in the matrix also occur.

Titanomagnetite–ilmenite intergrowths appear in the studied rocks, displaying trellis, sandwich (Fig. 2a–c) and composite types, as shown by Haggerty (1976, 1991). Trellis type is composed of ilmenite lamellae located along the {111} planes of the titanomagnetite host; sandwich type is defined by one or a small number of ilmenite laths along one set of the octahedral planes of the titanomagnetite, while the composite type consists of euhedral to anhedral ilmenite inclusions rarely orientated along {111} or {100} planes of the titanomagnetite, displaying contacts that may be sharp. These textures indicate a C2–C3 stage of high-temperature oxidation for our samples, as defined by Haggerty (1976, 1991).

Titanomagnetite replacement by titanohematite was a very common process in the studied samples. 'Martite' is the name given to the distinctive texture produced by pseudomorphic replacement of magnetite by hematite (Ramdohr 1980; Ixer & Duller 1998). While in some cases martitization only took place along the {111} planes of the titanomagnetite, in others it was strongly pervasive allowing a complete pseudomorphism.

Figure 2b shows two Fe–Ti oxide grains surrounding an iddingsitized olivine grain. The grains show ilmenite lamellae exsolved within

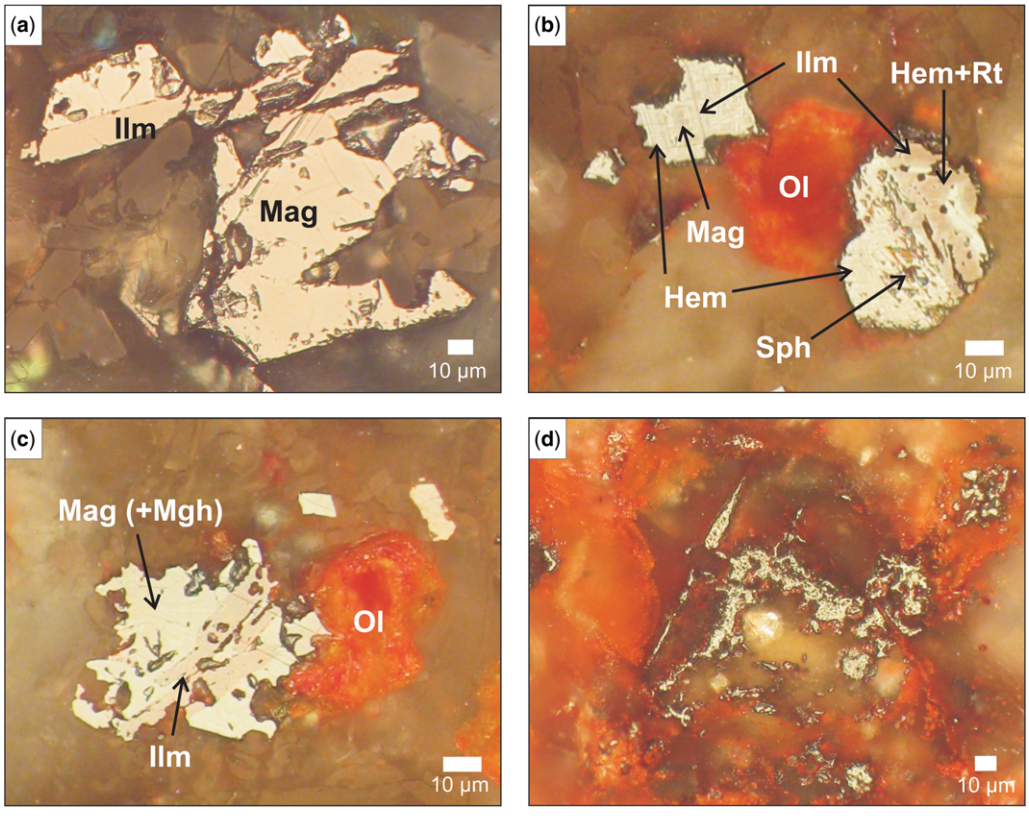

Fig. 2. Microphotographs of Fe–Ti oxides occurrences in Sierra de los Cóndores basalts, in reflected light and under oil immersion objectives. (**a**) N samples (EM4, site RU4-1 in Sierra de los Cóndores). Thick lath of ilmenite$_{ss}$ (Ilm) in sharply defined contact with optically homogeneous, octahedral (Ti)magnetite (Mag) defining a sandwich texture. C1 stage. (**b**) OX samples (EM30, site EST4 in Sierra de los Cóndores). Two Fe–Ti oxide grains surrounding an iddingsitized olivine (Ol) grain. Ilmenite is being altered to a fine mixture of titanohematite+rutile (pinkish lighter areas in the ilmenite, Hem+Rt), and (Ti)magnetite is highly altered to (Ti)maghemite+hematite (whitish pink–white, Hem+Mgh); incipient alteration to black sphene (Ttn). Small (Ti)magnetite islands remain as dark spots. (**c**) N samples (EP1, site D1 in El Pungo). A sandwich texture of ilmenite in (Ti)magnetite, highly corroded and close to an iddingsitized olivine. (**d**) HEM samples (RU34, clast in conglomerate). The original Fe-mineral is completely dissolved and only aggregates of granulated ilmenohematite remain. Note the intense reddening of the surrounding minerals by pigmentary, microcrystalline/amorphous Fe-oxide.

(Ti)magnetite (see the grain in the upper-left corner of Fig. 2b). The latter is highly altered to hematite (whitish pink–white). Hematite also forms lens-shaped patches (see the right-hand side of the crystal in the lower corner of Fig. 2b). Hematite could be a product of high-temperature oxidation (defining a C5 stage) or could result from low-temperature alteration.

Maghemitization is not easily detected in polished section unless it is sufficiently advanced to form shrinkage cracks. We just observed a variation in (Ti)magnetite of greyish-brown and whitish grey colours (Fig. 2c), interpreted as indicative of decomposition to (Ti)magnetite and (Ti)maghemite, respectively (Haggerty 1976). This observation was also confirmed by rock-magnetic experiments.

Besides martitization and maghemitization, the amygdaloidal samples (three lava flows, breccias and some of the basaltic clasts) may show also microcrystalline/amorphous Fe-oxides (limonite aggregates). In many cases, transformations of titanomagnetites are very advanced and only aggregates of granulated hematite$_{ss}$ remain (Fig. 2d).

However, ilmenite$_{ss}$ laths from sandwich intergrowths are also sometimes replaced, as shown in Figure 2b. A fine mixture of titanohematite + rutile (pinkish lighter areas in the ilmenite; see the right-hand side of the grain in the lower corner of

Fig. 2b) would attest to grade C5 high-temperature oxidation. Nevertheless, it should be taken into account that this assemblage can also be formed by low-temperature oxidation (e.g. Ade-Hall *et al.* 1971). Furthermore, black sphene may be also a product of ilmenite alteration at low temperatures. The assemblage may be interpreted as a product of high-temperature oxidation (grade C5) with subsequent low-temperature replacements, or as a combination of C2–C3 oxidation followed by low-temperature oxidation.

Ilmenite separate crystals mostly appear as tabular to acicular sections in the groundmass (mean length 0.05 mm, maximum of 0.15 mm). Rare microphenocrysts are only found in some trachyandesites. As in the laths of the intergrowths, ilmenite crystals also show replacements. Fine mixtures of hematite and rutile, both in the periphery and the central part of the crystals, were identified, indicating R5 stage alteration of Haggerty (1991) or low-temperature oxidation. A woven arrangement of light- and medium-grey phases replaces ilmenite in some crystals, presumably a mixture of Fe–Ti oxides formed at low temperatures (Ade-Hall *et al.* 1971).

It is important to take into account that the scale of alteration in opaque minerals varies considerably from grain to grain, probably as a result of oxidation disequilibrium.

It should be noted that a significant amount of hematite results from olivine alteration, as part of iddingsite. Iddingsite is a poorly crystalline mixture of smectite, chlorite and goethite/hematite formed by pseudomorphic replacement of olivine (e.g. Deer *et al.* 1982). Hematite may also appear as very small crystals around olivine. It also frequently appears as a scattered red, microcrystalline mineral phase formed by the oxidation of silicates, as described by Beske-Diehl & Li (1993).

Microprobe analyses were carried out on primary oxides of the studied rocks. Ulvöspinel molar per cents in the cubic phases (spinel series) mainly range from 50 to 85%; only in a small number of samples does the molar per cent range from 4 to 15% (Table 1, Fig. 3a). In the rhombohedral series, hematite molar per cents are low (6–8%), demonstrating that the phases are close to the ilmenite end member ($ilmenite_{ss}$), as shown in Table 1 and Figure 3a.

Coexistence of homogeneous phases from both series (magnetite–ilmenite pair) in the groundmass of a single sample allowed the temperature (T) and oxygen fugacity (fO_2) conditions during their formation to be determined, according to the method of Spencer & Lindsley (1981). Temperatures obtained vary from 845 to 1190 °C (Table 1). A T v. fO_2 diagram shows that samples lie on the quartz–magnetite–fayalite (QMF) buffer curve (Fig. 3b).

Hysteresis parameters

Three kinds of hysteresis loops were obtained for the 20 selected samples, reflecting significant variations in magnetization, coercive force and magnetic susceptibility (Figs 4 & 5, Table 2). A first group is dominated by a highly magnetic, low-coercivity mineral (Figs 4a & 5), presumably coarse-grained (Ti)magnetite in the pseudosingle domain (PSD) to multidomain (MD) range. We called this group 'N' because we consider the samples of this group to be representative of the minerals normally expected in fresh basalts. Virtually all of the less-evolved rocks of the alkaline suite and related groups (e.g. alkaline basalts, basanites, ankaratrites) show this magnetic behaviour, which correlates with high-Ti magnetite in the electron microprobe analyses.

A second group differs from the first one in having lower saturation magnetization, higher coercive force (Fig. 4b) and lower magnetic susceptibility (Fig. 5). All of these properties suggest a smaller effective grain size, typically produced by oxidation, as will be discussed later. Significantly, this group includes those samples with low-Ti magnetite in electron microprobe analyses. When compared with the theoretical SD+MD mixing curve of magnetite (shown in Fig. 5), the second group (named 'OX') coincides with a higher proportion of SD in the mixture. However, both groups deviate from the mixing curve to the right, suggesting that the magnetic assemblage includes more than a simple SD + MD magnetite mixture.

The 'OX' character occurs in the remaining lithological groups: transitional basalt, trachybasalt, latibasalt and trachyandesite. However, these lithologies are not exclusively OX, as they all experienced either N or OX behaviour, evidence of a further control on the magnetic properties in addition to lithology.

The third group (depicted in the inset in Fig. 5a) shows extremely high values of coercivity and low susceptibility, pointing to $hematite_{ss}$ as the main magnetic mineral (group 'HEM'), as is also indicated by the deviation to the right in the Day diagram (Fig. 5). Samples in this group are amygdaloidal samples with extreme reddening; the presence of abundant hematite in this highly porous material is a possible explanation of the observed magnetic properties. Hematite appears either as pigmentary ultrafine particles or as granulated aggregates (as in Fig. 2d).

Magnetic susceptibility

Bulk susceptibility is shown in Figure 6a along with saturation isothermal remanent magnetization for all of the 92 studied samples. We divided the

Table 1. *Magnetite and ilmenite microprobe compositions from selected rocks of Sierra Chica de Córdoba, in % of oxides*

Sample	G3	EM5	CO7	EM3	RU5	Li8	RU10B	PM4	PM1	PM7	PM6	MO1	Li1	ES2	Li4	CN1
Suite/Group	Bsn	AkB-Tc	AkB-Tc	AkB-Tc	AkB-Tc	AkB-Tc	AkB-Tc	AkB-Tc	AkB-Tc	AkB-Tc	AkB-Tc	AkB-Tc	TrB-Lb	TrB-Lb	TrB-Lb	TrB-Lb
Rock type	Bsn	AkB	Tcb	Tcb	Tca	Tca	Tca	AkB	Tca	Tcp	Tc	AkB	TrB	TrB	TrB	TrB
Site*	A4	RU4-1	TBNI	RU4-1	RU1-1	LIB4	RU1-5	Dyke	27–28	29–30	29–30	Dyke 14	LIB2	EST4	LIB3	A8
Locality	Pungo	Cónd.	Cónd.	Cónd.	Cónd.	Cónd.	Cónd.	Almaf.	Almaf.	Almaf.	Almaf.	Molinos	Cónd.	Cónd.	Cónd.	Cónd.
	gm	gm	gm	gm	gm	gm	gm	gm	gm	gm	gm	gm	gm	gm	gm	gm
Magnetite																
SiO_2	0.23	0.04	0.26	0.27	0.24	0.27	0.24	0.27	0.11	0.28	0.14	0.13	0.28	0.24	0.05	0.28
TiO_2	30.00	22.21	17.70	20.87	1.22	23.11	4.82	29.99	29.36	27.97	18.28	17.06	30.25	2.40	21.28	25.05
Al_2O_3	0.31	2.52	0.68	1.67	4.00	0.28	3.54	0.34	1.33	1.45	1.13	2.86	0.72	0.94	1.45	0.47
FeO_{total}	65.45	71.41	77.77	74.32	83.86	73.47	82.99	65.45	65.24	66.26	75.71	74.35	65.46	90.3	72.69	70.91
MnO	1.68	1.10	2.21	1.02	1.17	0.29	0.43	1.35	2.13	1.45	0.85	0.79	0.68	0.10	0.38	0.29
MgO	0.08	0.60	0.08	0.17	3.61	0.29	1.63	0.28	0.03	0.92	1.11	2.28	1.37	1.00	2.11	1.77
CaO	0.29	0.10	0.11	0.41	1.10	0.35	1.85	1.03	0.09	0.27	0.07	0.00	0.36	0.12	0.04	0.55
Cr_2O_3	0.05	0.21	0.00	0.01	0.00	0.15	0.00	0.08	0.13	0.00	0.02	0.06	0.07	0.00	0.49	0.00
Total	98.09	98.19	98.81	98.74	95.20	98.21	95.50	98.79	98.42	98.60	97.31	97.53	99.19	95.10	98.49	99.32
FeO	56.84	50.21	46.20	49.75	25.67	51.97	31.69	56.27	56.23	54.44	45.95	43.56	56.50	32.45	47.86	51.56
Fe_2O_3	9.57	23.55	35.07	27.29	64.66	23.89	57.00	10.20	10.01	13.14	33.06	34.21	9.96	64.28	27.59	21.50
Total	99.06	100.55	102.31	101.48	101.66	100.6	101.19	99.82	99.42	99.91	100.60	100.95	100.20	101.52	101.26	101.47
% Ulv.	85.92	62.82	50.19	59.35	4.28	65.88	14.48	85.10	83.69	79.43	51.85	48.03	85.05	7.70	59.17	69.78
Ilmenite																
SiO_2		0.24	0.01	0.06		0.15			0.03							
TiO_2		49.64	49.41	50.95		48.41			50.28							
Al_2O_3		0.79	0.00	0.04		0.2			0.25							
FeO_{total}		43.32	45.57	42.82		48.32			41.68							
MnO		0.87	0.70	0.83		0.23			2.52							
MgO		3.47	2.11	3.32		1.07			3.99							
CaO		0.11	0.06	0.14		0.20			0.17							
Cr_2O_3		0.06	0.00	0.03		0.23			0.01							
Total		0.00	0.00	98.19		0.00			0.00							
FeO		37.73	39.89	38.94		41.31			35.37							
Fe_2O_3		6.21	6.31	4.31		7.79			7.01							
Total		99.12	98.49	98.63		99.58			99.63							
% R_2O_3		7.04	6.00	4.14		7.93			6.88							
T (°C)		980	845	848		1040			1190							
log fO_2		−11.5	−14.1	−14.2		−10.4			−8.7							

*As in Geuna &Vizán (1998).

Bsn, basanite; AkB, alkali basalt; TrB, transitional basalt; Tcb, trachybasalt; Lb, latibasalt; AnB, andesi-basalt; Tca, trachyandesite; Tcp, trachyphonolite; Tc, trachyte; gm, microlite; Cónd., Sierra de los Cóndores; Almaf., Almafuerte locality. FeO, Fe_2O_3, R_2O_3 and Ulvöspinel (Ulv.) calculated according to Carmichael (1967). Temperature and log fO_2 following Spencer & Lindsley (1981) for homogenous magnetite–ilmenite pairs.

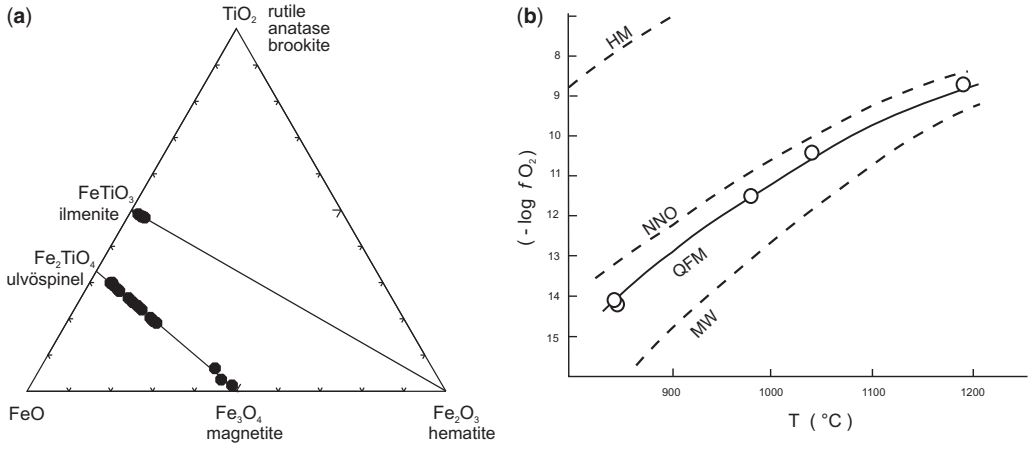

Fig. 3. (**a**) Ternary composition diagram of the $FeO–Fe_2O_3–TiO_2$ system for oxides from Sierra Chica de Córdoba, data from Table 1. Lines join end members of ülvospinel–magnetite and ilmenite–hematite solid solutions. $FeO = Fe^{2+} + Mg + Mn$, $Fe_2O_3 = 0.5\ (Fe^{3+} + Al + Cr)$, $TiO_2 = Ti$, according to Warner & Wasilewski (1997). (**b**) Temperature (°C) v. $-\log fO_2$ (Spencer & Lindsley 1981) for homogeneous groundmass magnetite–ilmenite pairs of Sierra Chica de Córdoba volcanic rocks (white dots are the magnetite–ilmenite pairs reported in Table 1). HM, hematite–magnetite; NNO, nickel–nickel oxide; FQM, fayalite–quartz–magnetite; MW, magnetite–wüstite.

samples into three groups according to the susceptibility values in such a way as to approximately coincide with the ranges observed for initial susceptibility in the hysteresis loops (groups in Fig. 5b). Figure 6a shows that group N is characterized by typical susceptibility values for basaltic rocks, whereas groups OX and HEM fall in a field below those normal values. While OX and HEM tend to cross the lines towards areas of smaller grain size for magnetite, the trend can be better explained by an assemblage composed of other minerals in addition to magnetite.

Imaginary (or out-of-phase) susceptibility (X'') was negligible for all but HEM samples. X'' for HEM samples was greater than 3° and up to 5°, and it was accompanied by frequency dependence (X_{fd}) of up to 12% and no field dependence (Table 2, see below). These characteristics are indicative of a short-period viscosity, and diagnostic for significant superparamagnetic/pseudosingle-domain presence (Hrouda *et al.* 2013).

IRM acquisition

The saturation isothermal remanent magnetization (SIRM) is the maximum intensity of remanence attained by samples when fields of 2.3 T were applied. The S ratio, designed to describe the relative contributions of high-coercive to low-coercive magnetic phases, has been calculated on the basis of the measurement of the backfield of the IRM. According to the definition of Bloemendal *et al.* (1992), it varies from 0 (for samples dominated by high-coercive phases) to 1 (for samples dominated by low-coercive phases).

The decreasing values of SIRM are accompanied by a decrease in the S ratio (Fig. 6b), which indicates that a high-coercivity mineral is being formed at

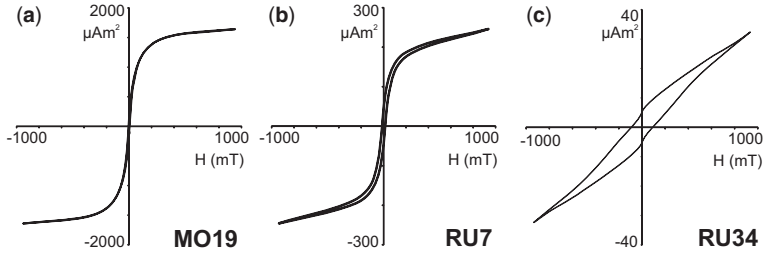

Fig. 4. Typical hysteresis loops. (**a**) N samples, MO19, dyke 4 in Los Molinos. (**b**) OX samples, RU7, basaltic clast in conglomerate. (**c**) HEM samples, RU34, amygdaloidal basaltic clast in conglomerate.

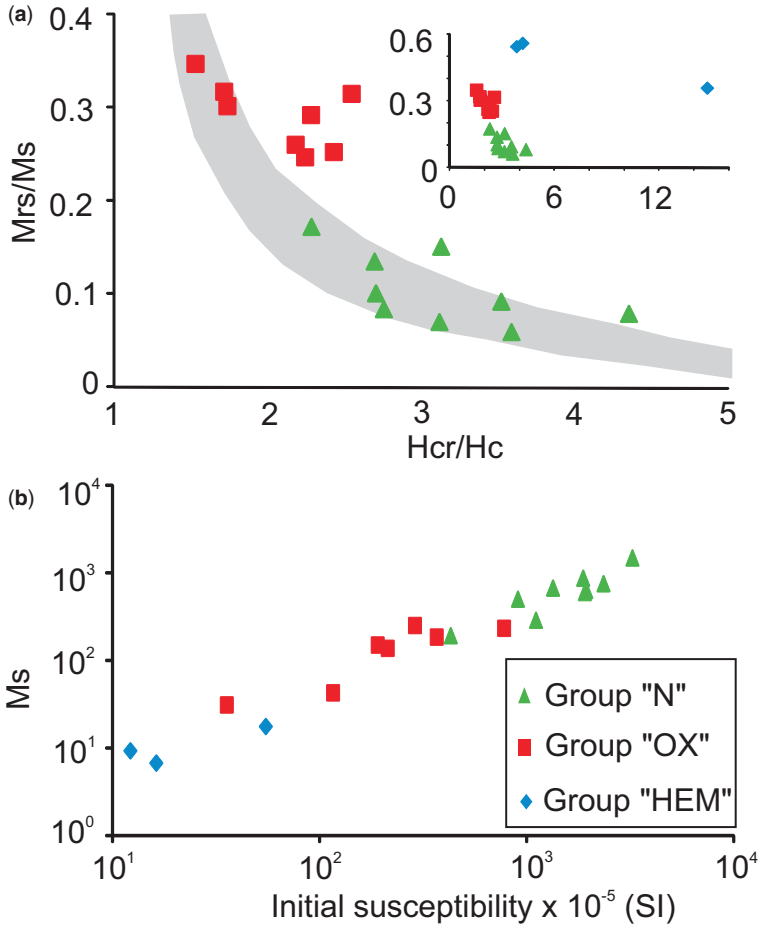

Fig. 5. (**a**), Hysteresis data on a Day-plot (Day *et al.* 1977); the theoretical SD + MD mixing curve of magnetite (after Dunlop 2002) is shown for comparison. (**b**), Saturation magnetization v. initial magnetic susceptibility from the hysteresis loop.

expense of the low-coercivity original (Ti)magnetite. The mean S ratio for magnetite-bearing rocks in group N is 0.96 (ranging between 0.87 and 1), while for OX rocks it is 0.86 (0.66–0.99) and, for HEM rocks, 0.46 (0.19–0.69: Table 2).

For most of the samples, two components of different coercivity coexist. Only five samples show a single component of the SIRM, which is (Ti)magnetite with coercivity of remanence (H_{cr}) varying between 10 and 35 mT. The remaining samples show composite IRM acquisition curves (Fig. 7). The analysis by cumulative log-Gaussian functions allows quantification of the amount of SIRM and the remanence–acquisition coercive force (H_{cr}) corresponding to each phase. Figure 8 shows the frequency distribution of coercivity values. Here, two main groups can be identified: a first group characterized by coercivity lower than 100 mT, presumably due to (Ti)magnetite/maghemite; and a second group characterized by coercivity higher than 200 mT and up to 1100 mT. Most of the high-coercivity component falls in the range 300–800 mT (hematite$_{ss}$?) with a few values above 1000 mT.

(Ti)magnetite/maghemite is dominant in most of the cases, complemented by hematite. The very-high coercivity component (>1000 mT) is always subordinate to the (Ti)magnetite component; it appears predominantly to be related to low-coercivity alkaline basalts, and might be due to the fine-grained hematite/goethite produced by alteration of olivine. The hematite component (coercivity 300–800 mT) is usually less than 25% of the SIRM but it can reach up to 70% in some samples.

Table 2. *Summary of magnetic properties of selected samples*

Sample	Site*	Location	Type	M_{rs} (mA m^2 kg^{-1})	M_s (mA m^2 kg $-$ ^{1})	H_{cr} (mT)	H_c (mT)	k ($\times 10^{-5}$ SI)	$k_{hf}/k^{\dagger}$	S ratio‡	$V^{\S}_{60/700}$	$X^{\|}_{fd}$	Curie temperature		IP¶
													First	Second	
PM1	27–28	Almaf.	N	57.3	605.6	12.0	3.4	1867	0.4	1.000	2.6				
PM5	31–33	Almaf.	N	29.8	193.9	32.3	10.3	421	1.6	0.954					
CN14	A1	Cónd.	N	54.6	881.6	13.7	3.8	1832	0.5						
EM4	RU4-1	Cónd.	N	55.5	763.5	11.5	3.7	2297	0.9	0.951	21.6	5.1	*c.* 420	560	-0.27**
LI1	LIB2	Cónd.	N	52.1	638.7	14.4	3.3	1897	0.6	0.934	1.7		*c.* 480	565	-0.35**
EM32	CC1	Cónd.	N	52.6	507.9	19.7	7.3	888	1.2	0.999	0.3	2.6	585		-0.66**
RU10	RU1b-1	Cónd.	N	93.8	681.0	21.5	8.0	1311	0.7	0.980	2.9	2.5	590		-0.69**
MO19	Dyke 4	Molinos	N	130.2	1504.6	13.2	4.8	3166	0.6	1.000	12.0	2.2	*c.* 450	580	-0.47**
EP1	D1	Pungo	N	51.0	291.5	11.9	5.2	1085	0.9	0.965	4.3		*c.* 450	550	
PM4	Dyke	Almaf.	OX	71.8	235.7	13.2	7.6	761	1.3	0.970	19.6		*c.* 390	580	-1.05**
RU5	RU1-1	Cónd.	OX	63.4	338.0	25.1	1.6	620	1.1		0.4	2.6	580		-0.33**
RU7	Clast	Cónd.	OX	46.8	187.4	32.8	14.6	360	2.8	0.897	0.9		*c.* 450	585	$-0.65^{\dagger\dagger}$
EM11	LIB4	Cónd.	OX	35.5	139.0	42.6	17.5	209	3.3	0.832	1.5		575		$-0.78^{\dagger\dagger}$
ES2	EST4	Cónd.	OX	66.8	253.7	47.4	21.7	283	3.7	0.942	0.2	1.7	580		$-0.35^{\dagger\dagger}$
CN3	A6 + 7 + 8	Cónd.	OX	44.8	151.8	51.2	22.4	187	5.2				575		
CO18	TBP	Cónd.	OX	10.0	31.3	72.7	28.5	35	26.0						
EM54	RU1-5	Cónd.	OX	13.8	43.1	14.6	8.5	114	4.7	0.397	2.9	2.7	365	520	$-0.15^{\dagger\dagger}$
EM50	Breccia	Cónd.	HEM	2.4	6.8	282.0	19.1	16	19.0	0.249	2.1	11.7			$0.44^{\dagger\dagger}$
RU34	Clast	Cónd.	HEM	5.2	9.3	384.0	92.0	12	34.0	0.301		11.7	605		
DS3	1	Despen	HEM	9.7	17.7	105.0	27.4	54	10.3	0.725	15.7		*c.* 420		$0.74^{\dagger\dagger}$

*As in Geuna & Vizán (1998).
†High-field susceptibility/total susceptibility from hysteresis loops.
‡S ratio as defined by Bloemendal *et al.* (1992): $S = (1 - IRM_{0.3T}/IRM_{1T})/2$.
§Dependence of X vs H calculated from fields 60/700 A m^{-1}.
$^{\|}X_{fd}$, frequency dependence of susceptibility calculated from frequencies 976/15 616 Hz.
¶IP irreversibility parameter from Böhnel *et al.* (2002).
**Ar atmosphere, 200 A m^{-1}.
††In air, 80 A m^{-1}.

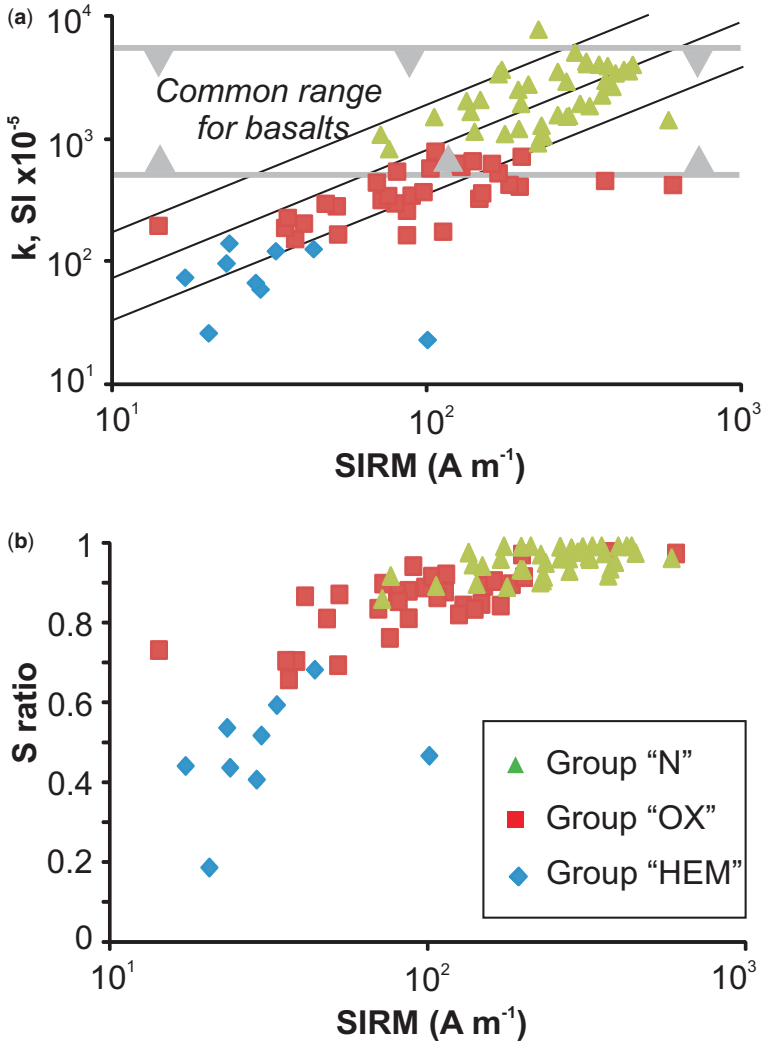

Fig. 6. Bilogarithmic plot v. SIRM of: (**a**) volume susceptibility (*k*). Sloping lines show an equal grain size for magnetite (from Thompson & Oldfield 1986). Common range of magnetic susceptibility for basalts is also shown after Clark (1999); (**b**) S ratio (Bloemendal *et al.* 1992) calculated from the IRM acquisition curve for the modelled components, based on Kruiver *et al.* (2001).

A rough estimation of mineral abundances can be attempted, considering the ranges of intrinsic magnetic remanence of saturation for magnetite, Ti-magnetite and maghemite (roughly 6 $Am^2 kg^{-1}$) v. that of hematite (roughly 0.2 $Am^2 kg^{-1}$: values after Peters & Dekkers 2003).

As hematite saturation magnetization is lower than magnetite by more than one order of magnitude, the observed relationships of SIRM imply that hematite is volumetrically more abundant than magnetite in most of the samples, with the most common association being around 2–10 times. This is consistent with the advanced degree of hematization of iron oxides observed in polished sections.

Thermomagnetic curves

Thermomagnetic curves of this study were systematically non-reversible, usually showing both a marked decrease in susceptibility and an increase in the Curie temperature during cooling. The Curie temperature was interpreted on the heating branch of the curve by the method of linear fit to inverse

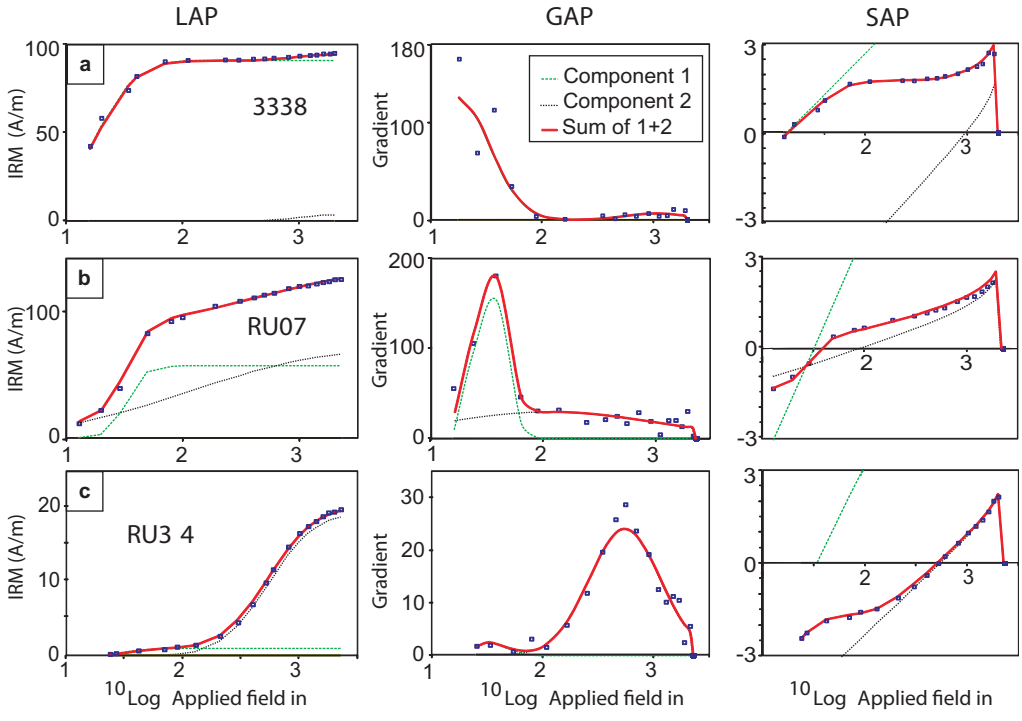

Fig. 7. IRM acquisition curves for previously demagnetized samples, shown as linear, gradient and standardized acquisition plots (LAP, GAP and SAP, respectively). The components modelled using the IRM–CLG 1.0 software (Kruiver *et al.* 2001) are shown. The abscissa is logarithmic for all three plots. (**a**) N samples, 3338, TCAS site in Sierra de los Cóndores. (**b**) OX samples, RU7, basaltic clast in conglomerate. (**c**) HEM samples, RU34, amygdaloidal basaltic clast in conglomerate.

susceptibility (Petrovský & Kapička 2006). However, this was not possible for more complicated curves due to superposition of several magnetic phases. In these cases only an approximation based on the peak method is provided.

The N samples showed typical curves of titanomagnetite, with asymmetrical peaks preceded by slightly convex low-temperature flanks (Moskowitz *et al.* 1998). The curves are non-reversible due to a shift in the Curie temperature to higher values in the cooling branch and also to a strong decrease in susceptibility (Fig. 9a, b). The Curie point determined from the first heating branch (most related to the original composition of the oxide) varied from 360 to 480 °C, being systematically higher than the expected values of −60 to 300 °C estimated from the electron microprobe analyses. The appearance of a Ti-poor magnetite phase during cooling is evident when heating in air (Fig. 9b). All of these features are indicative of a significant maghemitization of the titanomagnetite. The decrease in susceptibility would be related to the inversion of titanomaghemite to rhombohedral phases during heating (e.g. Doubrovine & Tarduno 2005; Lattard *et al.* 2006). Usually a single cycle of heating is enough to stabilize the oxide assemblage, the second heating cycle being reversible.

The OX samples also showed non-reversible behaviour with a significant loss of susceptibility on cooling, but the Curie temperatures were closer to that of pure magnetite, in a range from 500 to 590 °C (Fig. 9d). A subdued Verwey transition is observed at low temperatures, the virtual suppression of which might be due either to the Ti content or to non-stoichiometry of magnetite (Moskowitz *et al.* 1998). The increase in susceptibility with increasing temperature below about 400 °C is likely to be due to the gradual unblocking of superparamagnetic single-domain (SSD) particles. Some samples showed a wide range of Curie temperatures in the first heating cycle, followed by the development of two, more discrete, Curie temperatures revealed during cooling (Fig. 9c), which might be indicative of subsolidus exsolution, especially because this process has been observed to continue even in the second heating cycle (Fig. 9f).

Both increased Curie temperatures with respect to composition and strong non-reversibility in

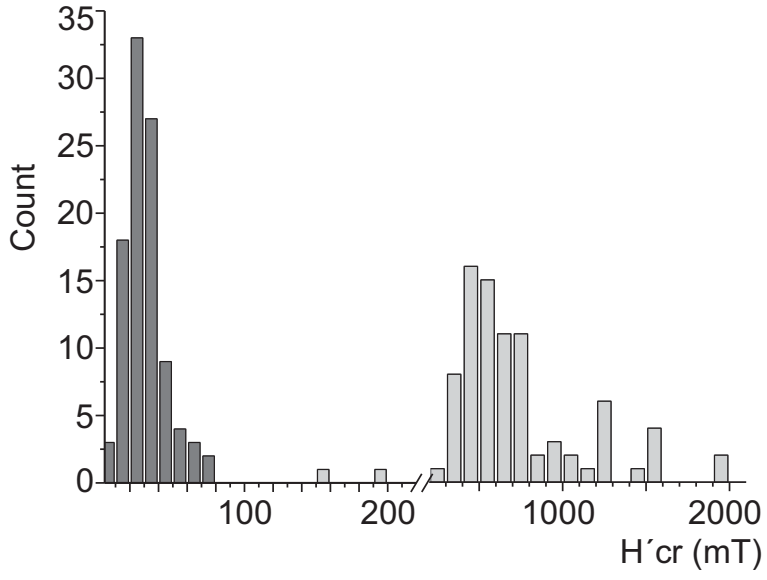

Fig. 8. H_{cr} distribution for the components of IRM determined in 92 samples; between one and three components were determined on each sample by modelling using the IRM–CLG 1.0 software (Kruiver *et al.* 2001). Note the change in the abscissa scale at 200 mT.

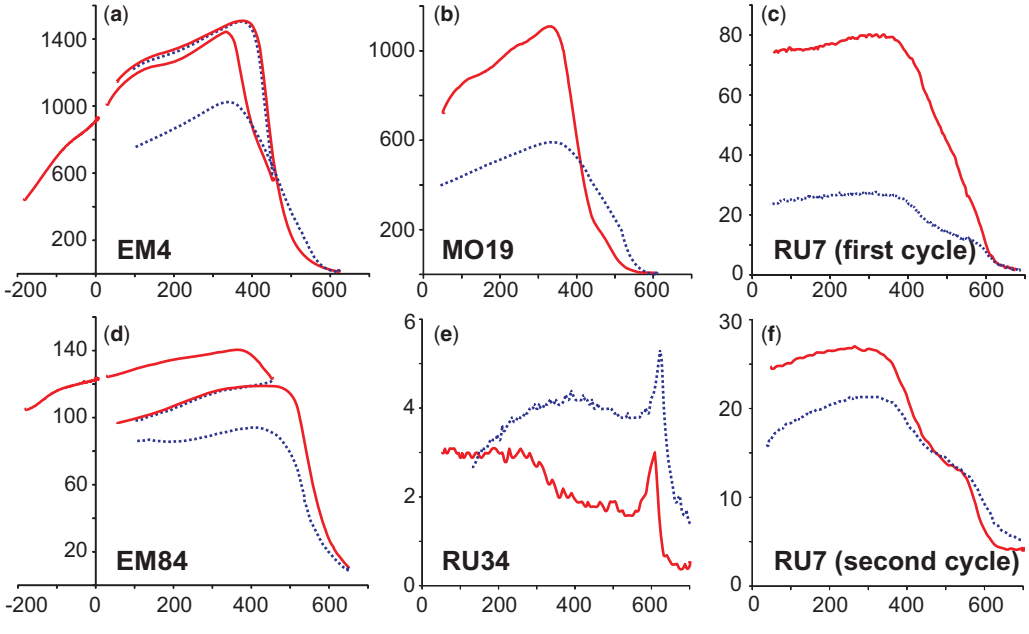

Fig. 9. Variation of magnetic susceptibility (arbitrary units) with temperature (T in °C). Full/dotted lines represent heating and cooling curves, respectively: (**a**) and (**d**) in Ar atmosphere with a MFK1 Agico Kappabridge (applied field 200 A m^{-1}); (**b**), (**c**), (**e**) and (**f**) in air with a MF2W Bartington susceptometer (applied field 80 A m^{-1}). (a) EM4, site RU4-1 in Sierra de los Cóndores (N sample). (b) MO19, dyke 4 in Los Molinos (N sample). (c) & (f) RU7, basaltic clast in conglomerate (OX sample). (d) EM84, site RU1-1 in Sierra de los Cóndores (OX sample). (e) RU34, amygdaloidal basaltic clast in conglomerate (HEM sample).

Curie temperatures are known to be related to cation vacancies (Lattard *et al.* 2006). Heating was accompanied by changes in the chemical composition – either related to oxidation or to unmixing by subsolvus exsolution of titanomagnetite – or in the degree of cation order of titanomagnetite, with the non-stoichiometric phases inverting to hematite$_{ss}$.

In spite of the abundant presence of hematite$_{ss}$ discussed in previous sections, it was not observed to contribute to the magnetic susceptibility of OX samples as the intrinsic susceptibility of hematite is several orders of magnitude less than magnetite/maghemite, and therefore the signal of magnetite/maghemite completely overwhelms that of hematite. That was not true for HEM samples, where the hematite/magnetite ratio is about 100:1; these samples showed the distinct signal of a Hopkinson peak at temperatures well over 600 °C (Fig. 9e). The observed Néel temperature was about 605–615 °C (i.e. lower than 675 °C), which means that hematite$_{ss}$ in these samples differs from the end-member hematite, probably containing a small amount of Ti.

Field dependence of magnetic susceptibility

It is known that alternating-current magnetic susceptibility of titanomagnetite is dependent on the applied field (e.g. Hrouda 2002). In the literature, a correlation between composition, expressed as Curie temperature, and the logarithm of the field-dependence parameter X_{Hd} has been proposed for alkaline volcanic rocks (de Wall 2000), with Ti-richest magnetites showing a dependence of more than 30%. Vahle & Kontny (2005) found that the correlation was also approximately valid for subaerial and submarine basalts in Hawaii, although systematic deviations were also observed and attributed to maghemitization.

Samples from Córdoba are characterized by low field-dependence of susceptibility (Fig. 10), in accordance with the high Curie temperatures. Both of these features indicate that the high Ti-content detected by electron microprobe is not representative of the effective magnetic mineralogy present in the sample. This discrepancy will be discussed later.

Demagnetization of the natural remanent magnetization

Geuna & Vizán (1998) studied the palaeomagnetism of these basalts and characterized their magnetic response to standard demagnetization techniques, such as alternating-field and thermal demagnetization. They found three magnetic components with different magnetic coercivities (named X, A and B), which were interpreted, respectively, as: a viscous magnetization carried by multidomain (Ti)magnetite (removed at no more than 30 mT); a chemical or thermochemical magnetization carried by fine (Ti)magnetite, possibly single or pseudosingle domain, formed by deuteric alteration (determined by alternating-field demagnetization between 30 and 100 mT); and a chemical

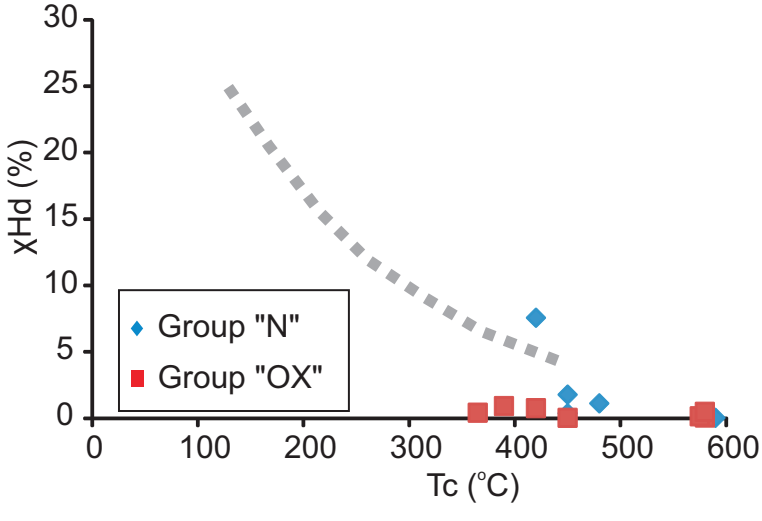

Fig. 10. Field dependence parameter X_{Hd} calculated from susceptibilities measured at 30 and 300 A m^{-1} plotted v. first Curie temperatures for basalts of groups N and OX. The dashed line indicates the regression line from de Wall (2000).

magnetization acquired by hematite$_{ss}$ (resistant to alternating-field demagnetization).

The three types of components were present in most of the samples in different proportions, and a relationship with oxidation was observed. Once the classification scheme of N, OX and HEM is applied to interpret the measurements of Geuna & Vizán (1998), a close correlation can be established between magnetic components and the three kinds of magnetic assemblages, as:

- Samples carrying only an X component were rare, and they were all N basalts. Usually N basalts carry a predominant X component along with a minor (1–10% of the natural remanent magnetization) A or B component. The median destructive field of these samples was lower than 10 mT (Fig. 11a), in coincidence with low H_{cr} determined for N samples.
- Samples carrying only an A component were all OX basalts. The median destructive field for these samples ranged between 10 and 25 mT when the A component was alone but it was increased up to 60 mT by the effect of a significant B component in some samples (Fig. 11b).
- Samples carrying only a B component were all HEM basalts.

While alternating-field demagnetization successfully separated components X and A, it could not remove the B component owing to its hardness, higher than the maximum equipment capability (130 mT). By contrast, thermal demagnetization was ineffective in separating components X and A, as their unblocking temperature spectra seemed to overlap. Eventual complexities in the B component (e.g. due to contributions of martite v. hematite from weathering) were also not defined because the range of unblocking temperatures exclusive for hematite is very narrow and the record becomes noisy at high temperatures because of the breakdown of minerals, which is accompanied by the generation of new magnetic phases.

The conglomerate test can provide valuable information about the timing, and therefore the possible origin, of each magnetic component. The clasts collected by Geuna & Vizán (1998) belong to the N, OX and HEM groups, and carried X, A and B components in variable proportions. The X component was not tested as it was observed to be viscous and randomly orientated even in the basaltic flows. For that reason, Geuna & Vizán (1998) classified the clasts into three types: (1) those recording only component A; (2) those recording both component A and component B; and (3) those recording only component B (Fig. 12).

A new examination of the demagnetization of clasts resulted in the scheme depicted in Figure 12. Many of the type (1) clasts not only recorded the A component but also contained a high-coercivity B component (Fig. 12a–c, e). The presence of the B component is interpreted from a significant portion of the remanence not removed with 130 mT. This component was overlooked by Geuna & Vizán (1998) because it is nearly coincident in direction with the lower-coercivity A component (Fig. 12a–c). The type (2) clasts of Geuna & Vizán (1998) also carried both components A and B but, in this case, they were easily identified because they had different directions (Fig. 12f).

As already noticed by Geuna & Vizán (1998), the A component was randomly orientated both in the type (1) and type (2) clasts (Fig. 12e, f), meaning that it was acquired before the lava flow was fragmented and the fragments transported to form the conglomerate. Regarding the B component, a new twist can be brought to its interpretation. Type (2) and (3) clasts record a B component with preferred orientation close to the post-Cretaceous magnetic field direction (Fig. 12d, f, g), while the B component in type (1) clasts is randomly orientated and very similar to the A component in the same clast (Fig. 12e). The contrasting behaviour is explained after examining the magnetic properties of the clasts: type (1) clasts are OX and N samples, while type (2) and (3) clasts are HEM samples with very low magnetic susceptibility and extreme reddening. This means that hematite due to weathering may be the magnetic carrier in clast types (2) and (3), providing a negative conglomerate test. However, the hematite-carrying component B in clasts type (1) would be mainly martite, formed by oxidation of the primary magnetic minerals. The conglomerate test implies that martitization occurred prior to fragmentation of the lava flow.

Discussion

Microprobe analyses on magnetite microphenocrysts show a content of about 50–85 mol% Usp, typical for tholeiitic and alkali basalts (Frost & Lindsley 1991). (Ti)magnetite with this composition is typical of fresh, young basaltic rocks; it should become paramagnetic at temperatures higher than 250 °C and its magnetic susceptibility should be strongly field-dependent (see Kontny *et al.* 2003; Vahle & Kontny 2005). The magnetic assemblage and magnetic properties observed for Sierra Chica de Córdoba basalts differ greatly from those expected in fresh basalts. This is not surprising as oxidation both at high and low temperatures is common in subaerial basalts, and causes drastic changes in magnetic mineralogy (e.g. Ade-Hall *et al.* 1971; Beske-Diehl & Li 1993; Dunlop & Özdemir 1997; Kontny *et al.* 2003).

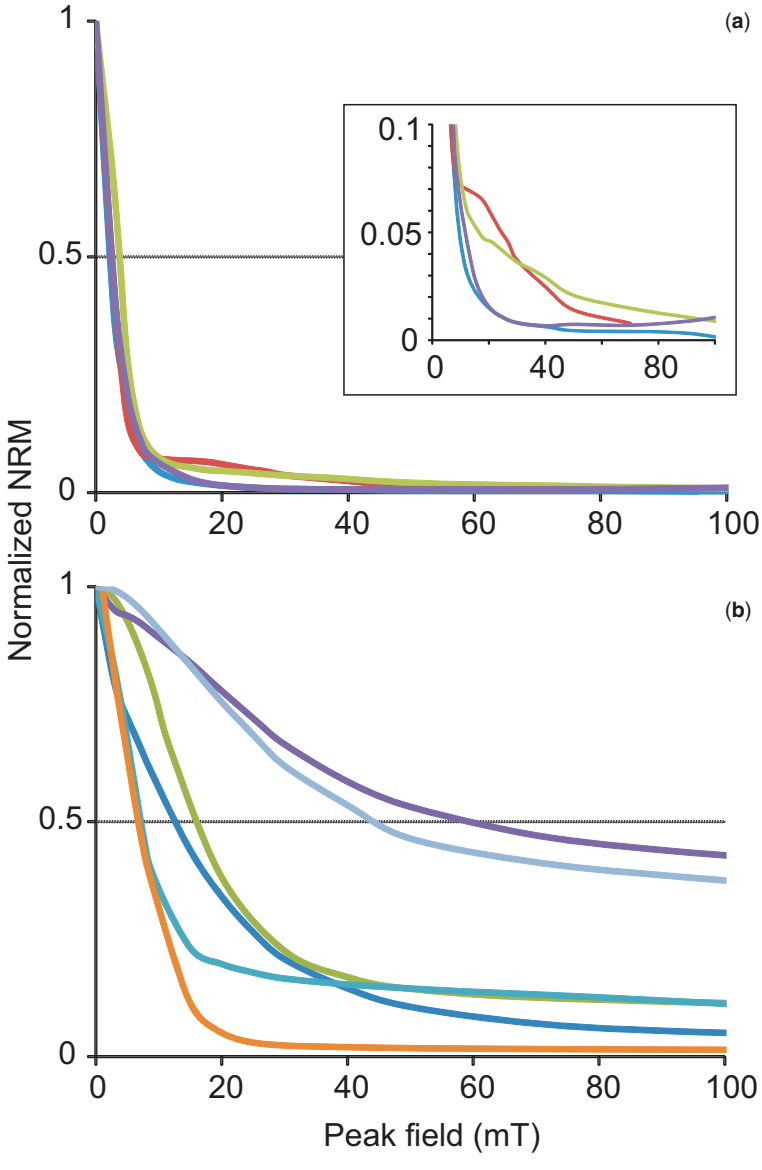

Fig. 11. Alternating-field (AF) demagnetization of the NRM, for: (**a**) N basalts; the inset shows the enlargement of the low-intensity region; and (**b**) OX basalts.

Palaeomagnetism and the timing of oxidation

Unravelling the oxidation sequence on a textural basis can sometimes be difficult, given that high- and low-temperature oxidation may lead to similar oxide assemblages. The possibility that martite and maghemite have been generated during a very late hydrothermal event should be evaluated. In order to do that, palaeomagnetic data and the results of the conglomerate test obtained by Geuna & Vizán (1998) were revisited taking into account the data acquired in this new study. First of all, we should establish the correlation between magnetic components and their magnetic carriers.

The subdued stable magnetization (A component) in N samples might have several carriers, as fine-grained magnetite produced by deuteric oxidation of olivine, fine exsolution blades and needles of magnetite in plagioclase/pyroxene (a common source of stable magnetization of basic rocks: e.g.

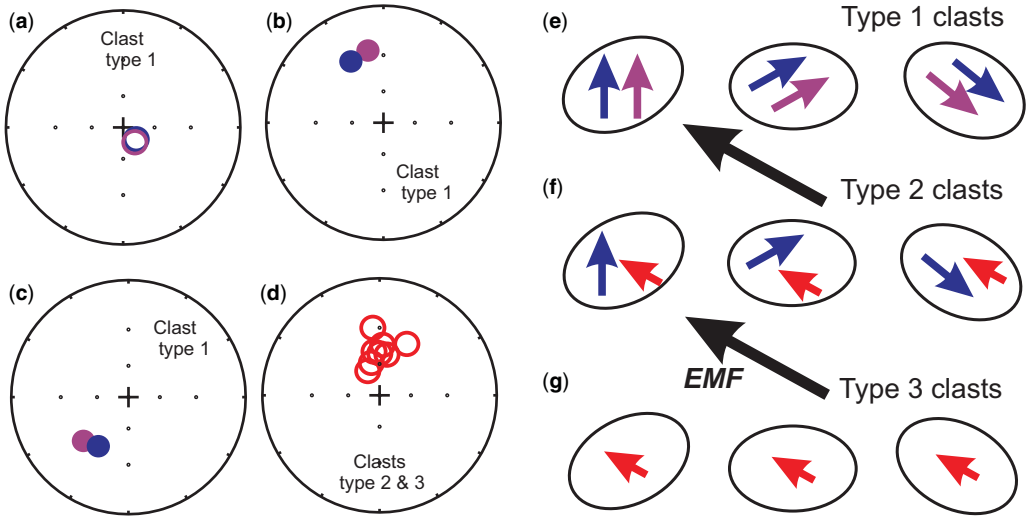

Fig. 12. Conglomerate test. The left-hand side of the figure depicts real palaeomagnetic data, while the right-hand side is a schematic interpretation. (**a**–**c**) Direction of components A (blue) and B (purple) in selected of type 1 clasts. (**d**) Direction of component B (red) in type 2 and 3 clasts. Open/full symbols are in the upper/lower hemisphere, respectively. (**e**–**g**) Schematic drawing showing the observed directions of magnetic remanence. (e) Each type 1 clast carries coincident A and B components (blue and purple arrows, see (a–c)), acquired before the conglomerate deposition. (f) Type 2 clasts carry an A component (blue arrow) acquired before, and a B component (red arrow) acquired after, conglomerate deposition. (g) Type 3 clasts carry only a B component aligned with the post-Cretaceous Earth's magnetic field (EMF) and therefore acquired after conglomerate deposition. While the B component in type 1 clasts is carried by martite (pseudomorphic hematite), the B component in type 2 and 3 clasts is carried by hematite produced by weathering. The natural remanent magnetization intensity of clasts type 3 is always <0.1 A m^{-1}.

Hargraves & Young 1969) or by the final products of oxidation of the large primary Fe–Ti oxides. In this respect, Figure 13 shows the correspondence between the degree of oxidation (as indicated by magnetic susceptibility) and the relative proportion of component A in the natural remanent magnetization. This proportion reaches values of nearly 100% in OX samples and is lower in the less oxidized N samples, which would suggest a relationship between the presence of A component and the degree of oxidation. The A component is clearly carried by oxidized/maghemitized, finely subdivided magnetite in OX samples; it may also be carried by a small fraction of non-stoichiometric (Ti)magnetite in N samples, although an additional contribution from very fine exsolution in silicates cannot be ruled out.

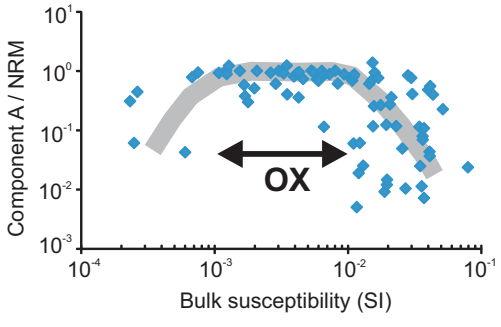

Fig. 13. Fraction of component A in the natural remanent magnetization (NRM), v. magnetic susceptibility. The arrow marks the approximate limits for the OX samples; for higher values of susceptibility (N samples), the NRM is increasingly the X component, while, for lower values (HEM samples), the NRM is increasingly the B component.

The A component, which dominates the magnetic remanence in OX samples, is carried by either single-domain (SD) magnetite or maghemite, according to the coercive force and unblocking temperatures. The remanence may be either a thermoremanent magnetization, if carried by SD-magnetite produced during high-temperature oxy-exsolution (higher than the Curie temperature of magnetite, *c.* 580 °C), or a chemical magnetization, if carried by maghemite formed at lower temperatures. Nonetheless, the new magnetic phases formed by maghemitization and/or submicroscopic grain division will have higher coercivity than original (Ti)magnetite, and therefore the magnetic remanence carried by them can easily be separated by AF demagnetization. By contrast, the unblocking

temperatures of both assemblages are expected to overlap completely, with (Ti)magnetite being gradually unblocked in a wide spectrum of temperatures, while maghemite is destroyed at temperatures even lower than 450 °C. This is precisely the scheme resulting from the demagnetization procedures by Geuna & Vizán (1998).

The A component in the basaltic clasts was acquired before the deposition of the conglomerate, which means that, even if the magnetization was acquired during low-temperature oxidation, it occurred very early, while volcanism was still active (as the conglomerate was followed by further lava flows). Therefore, it is a primary magnetization and can have a thermoremanent or a chemical origin. However, the B component is carried by hematite. Hematite is present in samples with two possible origins: (1) martitization and olivine alteration, both processes possibly occurring over a wide range of temperatures; and (2) granular aggregates produced during weathering. The conglomerate test showed that component B was acquired either before or after the fragmentation of lava flows, depending on the origin of the hematite. Samples with martite carried an early B component, while weathered (amygdaloidal) samples carried a late B component. It must be taken into account that the conglomerate formation is simultaneous with volcanism. This means that the B component in martite is not due to any hydrothermal event unrelated to the volcanic process. More likely, both maghemite and martite might be oxidation products in a process that may have proceeded up to hydrothermal temperatures in the presence of abundant, late magmatic fluids.

Oxidation features

Samples of Sierra Chica de Córdoba basalts show abundant evidence of oxidation in thin and polished sections. High-temperature oxidation seems evident in the development of the ilmenite lamellae with trellis texture that was observed in some samples, and which indicates formation at temperatures above 600 °C (e.g. Haggerty 1991). Other intergrowths such as sandwich and composite titanomagnetite–ilmenite grains can be either products of primary crystallization or subsequent high-temperature oxidation. The oxidation is not uniform, however, and in many samples magnetite is mostly relatively homogeneous.

As mentioned before, measured compositions of titanomagnetite and ilmenite homogeneous pairs in C1-grade samples indicate temperatures of formation ranging from 845 to 1190 °C. Interestingly, it should be noticed that most of the data are below 1100 °C (Table 1, Fig. 3), pointing to different stages of equilibration during post-eruptive quenching of the lavas (e.g. Bellieni *et al.* 1984). Taking into account these temperatures, most of the sandwich and composite intergrowths could have been formed by high-temperature oxidation processes in the deuteric stage. Furthermore, a deuteric origin would also explain the absence of graphic textures between ilmenite laths and the silicate matrix, a feature expected from primary crystallization in those textural arrangements according to Haggerty (1991).

Low-temperature oxidation (maghemitization) is widespread. Although optically it can only be identified by the inhomogeneous lightening in the colour of the replaced (Ti)magnetite, the magnetic properties are unequivocal. The thermomagnetic curves are non-reversible, with a significant reduction in the susceptibility on cooling and no changes in further heating cycles. (Ti)maghemite forms at low temperature and becomes unstable at temperatures higher than 450 °C (e.g. Lepp 1957), so the first heating should cause its inversion to the stable oxide form, hematite. In addition, the field dependence of the magnetic susceptibility is lower than expected according to the composition, and can even be suppressed. Maghemitization of (Ti)magnetite is the possible cause of the lower field dependence as it decreases the Fe^{2+} content and, therefore, the magnetocrystalline anisotropy of the Fe–Ti oxide (Vahle & Kontny 2005).

A significant feature of the Sierra Chica de Córdoba samples is the abundant presence of hematite as a magnetic carrier, as shown especially by the IRM acquisition curves and hysteresis loops, although it is not enough to dominate the magnetic properties due to the low intrinsic magnetization of hematite. The low-field thermomagnetic experiments fail to detect this unless its abundance is several orders greater than the magnetite abundance. The hematite is optically visible as a replacement product of magnetite (martitization) and olivine (iddingsitization); microcrystalline pigmentary Fe-oxide is also present. The most oxidized (HEM) samples show $hematite_{ss}$ as granulated aggregates, instead of martite or crystalline hematite.

The typical assemblages formed by oxidation are described below in five stages and schematized in Figure 14 in accordance with the theoretical depiction presented by O'Reilly (1984) and with the timing for remanence acquisition discussed above:

(1) *High-temperature non-stoichiometry.* A low grade of high-temperature (deuteric) oxidation leads to single-phase non-stoichiometric (Ti)magnetite. Only a limited degree of non-stoichiometry can be sustained, however, before (Ti)magnetite breaks up into an intergrowth of phases. This means that

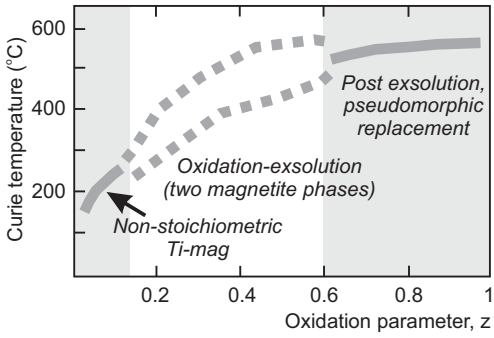

Fig. 14. Variation of the Curie temperature with bulk composition for deuterically oxidized titanomagnetite $Fe_{2.4}Ti_{0.6}O_4$ ($x = 0.6$, TM60), simplified from O'Reilly (1984). The Curie temperature is a single Curie point in the region of high-temperature non-stoichiometry, two Curie points (two titanomagnetites) in the exsolution stage of oxidation and one Curie point (magnetite) in the post-exsolution, pseudomorphic replacement stage. The oxidation process is accompanied by a decrease in magnetic susceptibility, and an increase in coercive force and M_{rs}/M_s ratio (e.g. O'Reilly 1984).

homogeneous, non-exsolved (Ti)magnetite can only be expected when the lava flow cooled quickly and/or with low oxygen pressure. This would be the case for our N samples, carrying apparently homogeneous (Ti)magnetite (at most in C2 stage) with a high Ti content according to the electron microprobe analyses. The Curie temperatures observed in low-field thermomagnetic curves for N samples, however, indicate that effective composition of the magnetic minerals is Ti-poorer than indicated by microprobe measurements, reaching at most Xusp = 0.3. This fact has to be explained by further transformations, as discussed in (4) below.

(2) *Oxidation–exsolution.* As oxidation proceeds, the original (Ti)magnetite becomes subdivided by lamellae of ilmenite, leading progressively to a titanium-depleted (Ti)magnetite. Samples are characterized by densely crowded exsolved ilmenite laths in a Ti-poor magnetite$_{ss}$ host, during a high-temperature oxidation up to stage C3 of Haggerty (1991). It is thought that the process takes place in nature at temperatures of 600–1150 °C, reproduced in the laboratory at 1275 °C (O'Reilly 1984). The well-known trellis texture is typically observed in some OX samples. Most of them are, therefore, characterized by the low Ti content of magnetite in electron microprobe analyses (ES2, RU5 and RU10A: see Table 1). The oxyexsolution is accompanied by an increase in coercivity and a decrease in magnetic susceptibility because of the grain-size reduction, as SD grains show lower susceptibility than MD grains (e.g. O'Reilly 1984). Low-field thermomagnetic curves show the presence of two magnetic phases with Curie temperatures of about 300–400 °C and closer to Ti-poor magnetite at about 580 °C, respectively (see Fig. 14), the latter being more abundant (Fig. 9c, d). At least part of the A component carried by the OX samples might have been acquired at this stage. However, some OX samples show a high Ti content in magnetite (e.g. PM4 and Li1: Table 2) showing that advanced oxyexsolution is not the only cause for the change in magnetic properties. A subsequent low-temperature oxidation to maghemite may occur, as suggested from optical observations and microprobe analysis (e.g. RU5, RU10B and ES2: Table 2), as will be discussed below.

(3) *Pseudomorphic replacement*. If the oxidation process goes further, once the Ti is completely exsolved, the stage of pseudomorphic replacement is reached (Fig. 14). At high temperature, titanomagnetite alters to hematite, while ilmenite alters to rutile plus titanohematite. This assemblage can represent stages C5 or R5 (for cubic and rhombohedral phases, respectively) attained at high temperatures. Nevertheless, it should be taken into account that an advanced oxidation process under low temperature would lead basically to the same products. However, the formation of black sphene from ilmenite laths (e.g. Fig. 2b) and the woven textural arrangement of titanium replacement of discrete ilmenite crystals, typical of low-temperature oxidation processes (e.g. Ade-Hall *et al.* 1971), also occur. Hence, hematite formation (martitization) seems to have occurred more probably under low-temperature conditions, along with iddingsitization, the generation of the scattered red mineral phase by silicate oxidation, and maghemitization. OX samples with pseudomorphic replacement show their magnetic susceptibility and remanence to be diminished. The magnetic remanence carried by martite was hard to recognize as a residual, subordinate component; when it was recognized, it was coincident with the component carried by the lower-coercive phase (magnetite/maghemite, Fig. 12), meaning that the process occurred early, possibly during cooling.

(4) *Low-temperature non-stoichiometry*. Oxidative alteration at low temperature (maghemitization) can produce a high degree of

non-stoichiometry, with significant effects on the magnetic remanence. The maghemitization causes an increase in the Curie temperature, a decrease in the intensity of magnetic remanence, saturation magnetization and magnetic susceptibility, and an increase in the stability of the magnetic remanence, either because of the mineral transformation or the reduction in size (Johnson & Hall 1978). Note that these effects are similar to those produced in (2). The discrepancy between microprobe and thermomagnetic measurements described for N samples in (1) is well known in oxidized basalts (e.g. Ade-Hall *et al.* 1965), and has been related to non-deuteric, hydrothermal alteration of Ti-rich titanomagnetite (Ade-Hall *et al.* 1971). Steinthorsson *et al.* (1992) referred to solvus exsolution of the magnetite$_{ss}$ leading to submicroscopic intergrowths (the cloth texture of Ramdohr 1953) to explain the paradox that, while magnetite contained a large amount of Ti, it behaved as a poor-Ti magnetite. Maghemitization occurred in both N and OX samples, and may well have represented a late stage of oxidation. It may be responsible for most (if not all) of the A component carried by these samples.

(5) *Weathering processes*. Chemical weathering by exposure near the Earth's surface causes the breakdown of Fe-bearing minerals to form hematite/goethite. The process is favoured when the exposure to external agents is greater: for example, in highly porous materials. Our HEM samples carry mostly granular hematite associated with maghemite and microcrystalline/amorphous Fe-oxides (limonite aggregates), which would be the product of extreme weathering in the amygdaloidal levels, volcanic breccias and the most weathered clasts. The magnetic remanence carried by HEM samples is coincident with the post-Cretaceous Earth's magnetic field, even in transported clasts, which proves that HEM samples acquired their remanence at a much later time.

Transition from monophasic to intergrown state to exsolution pseudomorphic replacement and maghemitization, implies an increase in Curie temperatures (as schematized in Fig. 14), a decrease in susceptibility, and a gradual increase in both the coercive force and the ratio of saturation remanence to saturation magnetization (M_{rs}/M_s) in magnetic minerals. All these features were observed in our OX samples.

It seems clear that the groups identified on the basis of magnetic properties (N, OX and HEM) represent increasing grades of oxidation, regardless of its origin, and in accordance with microscopic mineralogical and textural features. The characteristic remanent magnetization is seldom carried by the primary, igneous assemblage. Instead, it seems to be carried by minerals produced during deuteric oxidation, whether at high temperature (the classical assemblages C2–C5 described by Haggerty 1976, 1991) or at lower temperatures (maghemitization + martitization). The oxidation caused a lowering of the effective magnetic grain size, therefore enhancing the magnetic stability.

The lithology exerts a crude control, as all primitive alkaline lithologies (basanites, ankaratrites and alkaline basalts) showed N behaviour. However, the remaining samples experienced either N or OX behaviour irrespective of the lithology, evidence of a further control on the magnetic properties. While N basalts experienced a low grade of high-temperature oxidation (C1–C2), OX samples suffered high-temperature oxidation in grade C3 (possibly up to C5), which partly explains the differences in the magnetic properties, and must be due to different amounts of fluids in each particular lava flow. Both groups show evidence of widespread martitization and maghemitization, which would have occurred at lower temperatures, in an environment of high fluid circulation. Even samples that were not highly oxidized at high temperatures (N samples) experienced maghemitization. Local evidence of late-stage, low-temperature oxidation comes from zeolite minerals infilling vesicles in some lava flows in Sierra de los Cóndores, which indicate temperatures $<300\ ^{\circ}C$ (Lagorio & Montenegro 1996).

The palaeomagnetic evidence, however, suggests that the stable magnetic remanence, probably carried by maghemite, was acquired early, coevally with volcanism, which means that hydrothermal activity was linked to the volcanic event and, therefore, the magnetic remanence can be considered essentially primary. For the most oxidized flows ('brown basalts' of Gordillo & Lencinas 1967*a*, mostly our OX samples), the high- and low-temperature oxidation might have been a continuous process recorded during the first cooling in the presence of abundant late magmatic fluids. However, the least oxidized levels ('black basalts' of Gordillo & Lencinas 1967*a*, our N samples) might have been altered by the reheating of the lower flows by successive ones. Galindo *et al.* (1997) described the long-lived, high-level convective circulation of hot hydrothermal fluids (215–300 °C) in Córdoba during the Cretaceous, giving rise to fluorite lodes. The magnetic assemblage observed would be consistent with cooling in such a geothermal system.

This has a number of implications for the palaeomagnetic record. The remanence most probably records the Earth's magnetic field direction at the time of cooling or very soon after, which means that it still can be used for geodynamic purposes. However, the complexity in the acquisition and the possibility of prompt resetting, means that the flow succession could not faithfully record the palaeosecular variation of the Earth's magnetic field. Furthermore, the part of the magnetic remanence acquired below the Curie temperature through the maghemitization process would be a chemical–thermochemical remanence, not obeying the laws of thermoremanence acquisition. This implies that, if maghemitization plays a role in the remanence acquisition, the intensity of the acquired remanence would have little connection to the palaeointensity of the Earth's magnetic field. This explains the scarce results obtained by Cejudo-Ruiz *et al.* (2006), who only found acceptable palaeointensity results in a few isolated lava flows from the Sierra de los Cóndores Group.

Lastly, HEM samples would result from the effects of late (possibly very recent), extreme weathering due to their high porosity.

Conclusions

Three different groups of magnetic behaviour can be identified in the Sierra Chica de Córdoba subaerial mildly alkaline to transitional Cretaceous basalts, related to the degree of high-temperature oxidation during the lava extrusion, combined with superimposed low-temperature maghemitization and hematization. They represent increasing grades of oxidation.

Our data suggest that the characteristic remanent magnetization was mostly acquired during deuteric/hydrothermal oxidation, in a temperature range that could have gone below Curie temperatures. However, palaeomagnetic and geological evidence support an early acquisition, implying that oxidation occurred immediately after emplacement, possibly as part of the cooling process in the presence of residual fluids. Despite being a thermochemical–chemical magnetization, the characteristic remanence may be considered as primary.

The observed magnetic assemblage requires cooling in the presence of fluids. The scheme of maghemitization followed by slow, late hematization is coincident with that proposed by Steinthorsson *et al.* (1992) for the oxidation of Icelandic basalts, in the frame of a low-temperature geothermal system. The alteration produced under these conditions caused the stabilization of the magnetic remanence, creating suitable conditions for palaeomagnetic studies. However, when the oxidizing conditions were extreme, as in amygdaloidal zones of thin flows and breccias, destruction of magnetic minerals and loss of original magnetization occurred.

We thank the editors, D. Clark, J. Bowles and an anonymous reviewer for their constructive comments that helped us to improve the manuscript. This work was partially supported by grants from ANPCyT (PICT–2011–0956), UBACyT (20020100100047 and 20020110100064) and CONICET (PIP 112–200801–01502 and 112–201101–00294). R. Somoza and M. Iacumin provided assistance with the fieldwork. R. Siqueira kindly helped during the laboratory work in Sao Paulo and provided the software to analyse hysteresis loops. Special thanks to G. Bellieni, who generously provided the electron microprobe analyses at the University of Padova.

References

Ade-Hall, J. M., Wilson, R. L. & Smith, P. J. 1965. The petrology, Curie points and natural magnetizations of basic lavas. *Geophysical Journal of the Royal Astronomical Society*, **9**, 323–335, http://dx.doi.org/10.1111/j.1365-246X.1965.tb03890.x

Ade-Hall, J. M., Palmer, H. C. & Hubbard, T. P. 1971. The magnetic and opaque petrological response of basalts to regional hydrothermal alteration. *Geophysical Journal of the Royal Astronomical Society*, **24**, 137–174, http://dx.doi.org/10.1111/j.1365-246X.1971.tb02171.x

Alt, J. C. 1998. Very low-grade hydrothermal metamorphism of basic igneous rocks. *In*: Frey, M. & Robinson, D. (eds) *Low-Grade Metamorphism*. Blackwell Science, Oxford, 169–226, http://dx.doi.org/10.1002/9781444313345.ch6

Bellieni, G., Comin-Chiaramonti, P., Marques, L. S., Melfi, A. J., Piccirillo, E. M., Nardy, A. J. & Roisemberg, A. 1984. High- and low-TiO2 flood basalts from the Paraná plateau (Brazil): petrology and geochemical aspects bearing on their mantle origin. *Neues Jahrbuch für Mineralogie Abhandlungen*, **150**, 273–306.

Beske-Diehl, S. & Li, H. 1993. Magnetic properties of hematite in lava flows from Iceland: response to hydrothermal alteration. *Journal of Geophysical Research*, **98**, 403–417, http://dx.doi.org/10.1029/92JB01253

Bloemendal, J., King, J. W., Hall, F. R. & Doh, S. J. 1992. Rock magnetism of Late Neogene and Pleistocene deep-sea sediments: relationship to sediment source, diagenetic processes and sediment lithology. *Journal of Geophysical Research*, **97**, 4361–4375, http://dx.doi.org/10.1029/91JB03068

Böhnel, H., McIntosh, G. & Sherwood, G. 2002. A parameter characterising the irreversibility of thermomagnetic curves. *Physics and Chemistry of the Earth*, **27**, 1305–1309, http://dx.doi.org/10.1016/S1474-7065(02)00124-9

Buddington, A. F. & Lindsley, D. H. 1964. Iron-titanium oxide minerals and synthetic equivalents. *Journal of Petrology*, **5**, 319–357, http://dx.doi.org/10.1093/petrology/5.2.310

Carmichael, I. S. E. 1967. The iron-titanium oxides of salic volcanic rocks and their associated ferromagnesian silicates. *Contributions to Mineralogy and Petrology*, **14**, 36–63, http://dx.doi.org/10.1007/BF00370985

Cejudo-Ruiz, R., Goguitchaichvili, A., Geuna, S. E., Alva-Valdivia, L., Solé, J. & Morales, J. 2006. Early Cretaceous absolute geomagnetic paleointensities from Córdoba province (Argentina). *Earth, Planets and Space*, **58**, 1333–1339.

Clark, D. A. 1999. Magnetic petrology of igneous intrusions: implications for exploration and magnetic interpretation. *Exploration Geophysics*, **30**, 5–26, http://dx.doi.org/10.1071/EG999005

Cui, Y., Verosub, K. L. & Roberts, A. P. 1994. The effect of low-temperature oxidation on large multi-domain magnetite. *Geophysical Research Letters*, **21**, 757–760, http://dx.doi.org/10.1029/94GL00639

Day, R., Fuller, M. D. & Schmidt, V. A. 1977. Hysteresis properties of titanomagnetites: Grain size and composition dependence. *Physics of the Earth and Planetary Interiors*, **13**, 260–267, http://dx.doi.org/10.1016/0031-9201(77)90108-X

Deer, W. A., Howie, R. A. & Zussman, J. 1982. *Rock-Forming Minerals. Volume 1A, Orthosilicates*. Longman, London.

de Wall, H. 2000. The field-dependence of AC susceptibility in titanomagnetites: implications for the anisotropy of magnetic susceptibility. *Geophysical Research Letters*, **27**, 2409–2411, http://dx.doi.org/10.1029/2000GL008515

Doubrovine, P. V. & Tarduno, J. A. 2005. On the compositional field of self-reversing titanomaghemite: constraints from Deep Sea Drilling Project Site 307. *Journal of Geophysical Research*, **110**, B11104, http://dx.doi.org/10.1029/2005JB003865

Dunlop, D. J. 2002. Theory and application of the Day plot (Mrs/Ms versus Hcr/Hc) 1. Theoretical curves and tests using titanomagnetite data. *Journal of Geophysical Research*, **107**, B3, http://dx.doi.org/10.1029/2001JB000486

Dunlop, D. J. & Özdemir, Ö. 1997. *Rock Magnetism. Fundamentals and Frontiers*. Cambridge University Press, Cambridge, http://dx.doi.org/10.1017/CBO9780511612794

Frost, B. R. & Lindsley, D. H. 1991. Occurrence of iron-titanium oxides in igneous rocks. *In*: Lindsley, D. H. (ed.) *Oxide Minerals: Petrologic and Magnetic Significance*. Reviews in Mineralogy, **25**. Mineralogical Society of America, Chantilly, VA, 433–468.

Galindo, C., Pankhurst, R. J., Casquet, C., Coniglio, J., Baldo, E., Rapela, C. W. & Saavedra, J. 1997. Age, Sr- and Nd-isotope systematics, and origin of two fluorite lodes, Sierras Pampeanas, Argentina. *International Geology Review*, **39**, 948–954, http://dx.doi.org/10.1080/00206819709465312

Geuna, S. E. & Vizán, H. 1998. New Early Cretaceous palaeomagnetic pole from Córdoba Province (Argentina): revision of previous studies and implications for the South American database. *Geophysical Journal International*, **135**, 1085–1100, http://dx.doi.org/10.1046/j.1365-246X.1998.00688.x

Gordillo, C. E. & Lencinas, A. 1967*a*. Geología y petrología del extremo norte de la Sierra de Los Cóndores, Córdoba. *Boletín Academia Nacional de Ciencias*, **46**, 73–108.

Gordillo, C. E. & Lencinas, A. 1967*b*. El basalto nefelínico de El Pungo, Córdoba. *Boletín Academia Nacional de Ciencias*, **46**, 109–115.

Gordillo, C. E. & Lencinas, A. 1969. Perfil geológico de la sierra Chica de Córdoba en la zona del río Los Molinos, con especial referencia a los diques traquibasálticos que la atraviesan. *Boletín Academia Nacional de Ciencias*, **47**, 27–50.

Gordillo, C. E. & Lencinas, A. 1980. Sierras Pampeanas de Córdoba y San Luis. *In*: Turner, J. C. M. (ed.) *Segundo Simposio de Geología Regional Argentina*, Vol. **1**. Academia Nacional de Ciencias, Córdoba, 577–650.

Haggerty, S. E. 1976. Opaque mineral oxides in terrestrial igneous rocks. *In*: Rumble, D. III (ed.) *Oxide Minerals*. Reviews in Mineralogy, **3**. Mineralogical Society of America, Chantilly, VA, 101–300.

Haggerty, S. E. 1991. Oxide textures – a mini-atlas. *In*: Lindsley, D. H. (ed.) *Oxide Minerals: their Petrologic and Magnetic Significance*. Reviews in Mineralogy, **25**. Mineralogical Society of America, Chantilly, VA, 29–220.

Hall, J. M. 1985. The Iceland Research Drilling Project crustal section: variation of magnetic properties with depth in Icelandic-type oceanic crust. *Canadian Journal of Earth Sciences*, **22**, 85–101, http://dx.doi.org/10.1139/e85-007

Hargraves, R. B. & Young, W. M. 1969. Source of stable remanent magnetism in Lambertville diabase. *American Journal of Science*, **267**, 1161–1167, http://dx.doi.org/10.2475/ajs.267.10.1161

Hrouda, F. 2002. Low-field variation of magnetic susceptibility and its effect on the anisotropy of magnetic susceptibility of rocks. *Geophysical Journal International*, **150**, 715–723, http://dx.doi.org/10.1046/j.1365-246X.2002.01731.x

Hrouda, F., Pokorný, J., Ježek, J. & Chadima, M. 2013. Out-of-phase magnetic susceptibility of rocks and soils: a rapid tool for magnetic granulometry. *Geophysical Journal International*, **194**, 170–181, http://dx.doi.org/10.1093/gji/ggt097

Ixer, R. A. & Duller, P. R. 1998. *Virtual Atlas of Opaque and Ore Minerals and their Associations*. Version 1.1b. http://www.smenet.org/opaque-ore/

Johnson, H. P. & Hall, J. M. 1978. A detailed rock magnetic and opaque mineralogy study of the basalts from the Nazca plate. *Geophysical Journal of the Royal Astronomical Society*, **52**, 45–64, http://dx.doi.org/10.1111/j.1365-246X.1978.tb04221.x

Kay, S. M. & Ramos, V. A. 1996. El magmatismo cretácico de las sierras de Córdoba y sus implicancias tectónicas. *Actas 13° Congreso Geológico Argentino y 3 Congreso de Exploración de Hidrocarburos, Buenos Aires*, **3**, 453–464.

Kontny, A., Vahle, C. & de Wall, H. 2003. Characteristic magnetic behavior of subaerial and submarine lava units from the Hawaiian Scientific Drilling Project (HSDP-2). *Geochemistry, Geophysics, Geosystems*, **4**, 8703, http://dx.doi.org/10.1029/2002GC000304

Kraemer, P. E., Escayola, M. P. & Martino, R. D. 1995. Hipótesis sobre la evolución tectónica neoproterozoica de las Sierras Pampeanas de Córdoba (30°40′–32°40′),

Argentina. *Revista de la Asociación Geológica Argentina*, **50**, 47–59.

KRUIVER, P. P., DEKKERS, M. J. & HESLOP, D. 2001. Quantification of magnetic coercivity components by the analysis of acquisition curves of isothermal remanent magnetisation. *Earth and Planetary Science Letters*, **189**, 269–276, http://dx.doi.org/10.1016/S0012-821X(01)00367-3

LAGORIO, S. L. 2008. Early Cretaceous alkaline volcanism of the Sierra Chica de Córdoba (Argentina): mineralogy, geochemistry and petrogenesis. *Journal of South American Earth Sciences*, **26**, 152–171, http://dx.doi.org/10.1016/j.jsames.2008.05.003

LAGORIO, S. L. & MONTENEGRO, T. F. 1996. Ceolita de la serie analcima-wairakita en el cerro Libertad, Sierra de los Cóndores, Córdoba. *In*: BRODTKORB, M. & SCHALAMUK, I. (eds) *3° Reunión de Mineralogía y Metalogenia*. Instituto de Recursos Minerales, Universidad Nacional de La Plata, Publicación, **5**, 139–146.

LANZA, R. & ZANELLA, E. 1993. Palaeomagnetism of the Ferrar dolerite in the northern Prince Albert Mountains (Victoria Land, Antarctica). *Geophysical Journal International*, **114**, 501–511, http://dx.doi.org/10.1111/j.1365-246X.1993.tb06983.x

LATTARD, D., ENGELMANN, R., KONTNY, A. & SAUERZAPF, U. 2006. Curie temperatures of synthetic titanomagnetites in the Fe-Ti-O system: effects of composition, crystal chemistry, and thermomagnetic methods. *Journal of Geophysical Research*, **111**, B12S28, http://dx.doi.org/10.129/2006JB004591

LEPP, H. 1957. Stages in the oxidation of magnetite. *American Mineralogist*, **42**, 679–681.

LINARES, E. & GONZÁLEZ, R. 1990. *Catálogo de edades radimétricas de la República Argentina, 1957–1987*. Publicaciones Especiales de la Asociación Geológica Argentina, Serie B (Didáctica y Complementaria), **19**.

LINARES, E. & VALENCIO, D. A. 1975. Paleomagnetism and K–Ar ages of some trachybasaltic dykes from Río Los Molinos, Province of Córdoba, Republic of Argentina. *Journal of Geophysical Research*, **80**, 3315–3321, http://dx.doi.org/10.1029/JB080i023 p03315

MENDÍA, J. E. 1978. Paleomagnetic study of alkaline vulcanites from Almafuerte, province of Cordoba, Argentina. *Geophysical Journal of the Royal Astronomical Society*, **54**, 539–546, http://dx.doi.org/10.1111/j.1365-246X.1978.tb05493.x

MOSKOWITZ, B. M., JACKSON, M. & KISSEL, C. 1998. Low temperature magnetic behavior of titanomagnetites. *Earth and Planetary Science Letters*, **157**, 141–149, http://dx.doi.org/10.1016/S0012-821X(98)00033-8

OLIVA-URCIA, B., KONTNY, A., VAHLE, C. & SCHLEICHER, A. M. 2011. Modification of the magnetic mineralogy in basalts due to fluid-rock interactions in a high-temperature geothermal system (Krafla, Iceland). *Geophysical Journal International*, **186**, 155–174, http://dx.doi.org/10.1111/j.1365-246X.2011.05029.x

O'REILLY, W. 1984. *Rock and Mineral Magnetism*. Blackie, Glasgow, http://dx.doi.org/10.1007/978-1-4684-8468-7

PETERS, C. & DEKKERS, M. J. 2003. Selected room temperature magnetic parameters as a function of mineralogy, concentration and grain size. *Physics and Chemistry of the Earth*, **28**, 659–667, http://dx.doi.org/10.1016/S1474-7065(03)00120-7

PETROVSKÝ, E. & KAPIČKA, A. 2006. On determination of the Curie point from thermomagnetic curves. *Journal of Geophysical Research*, **111**, B12S27, http://dx.doi.org/10.1029/2006JB004507

PRÉVOT, M., MATTERN, E., CAMPS, P. & DAIGNIÈRES, M. 2000. Evidence for a 20° tilting of the Earth's rotation axis 110 million years ago. *Earth and Planetary Science Letters*, **179**, 517–528, http://dx.doi.org/10.1016/S0012-821X(00)00129-1

RAMDOHR, P. 1953. Ulvöspinel and its significance in titaniferous iron ores. *Economic Geology*, **48**, 677–688, http://dx.doi.org/10.2113/gsecongeo.48.8.677

RAMDOHR, P. 1980. *The Ore Minerals and their Intergrowths*. Pergamon Press, Oxford.

RAMOS, V. A., ESCAYOLA, M. P., MUTTI, D. I. & VUJOVICH, G. I. 2000. Proterozoic-early Paleozoic ophiolites of the Andean basement of southern South America. *In*: DILEK, Y., MOORES, E. M., ELTHON, D. & NICHOLAS, A. (eds) *Ophiolites and Oceanic Crust: New Insights from Field Studies and the Ocean Drilling Program*. Geological Society of America, Special Papers, **349**, 331–349, http://dx.doi.org/10.1130/0-8137-2349-3.331

ROBERTSON, D. J. & FRANCE, D. E. 1994. Discrimination of remanence-carrying minerals in mixtures, using isothermal remanent magnetisation acquisition curves. *Physics of the Earth and Planetary Interiors*, **82**, 223–234, http://dx.doi.org/10.1016/0031-9201(94)90074-4

ROBINSON, D. & BEVINS, R. E. 1998. Patterns of regional low-grade metamorphism in metabasites. *In*: FREY, M. & ROBINSON, D. (eds) *Low-Grade Metamorphism*. Blackwell Science, Oxford, 143–168, http://dx.doi.org/10.1002/9781444313345.ch5

SCHMIDT, C. J., ASTINI, R. A., COSTA, C. H., GARDINI, C. E. & KRAEMER, P. E. 1995. Cretaceous rifting, alluvial fan sedimentation and Neogene inversion, southern Sierras Pampeanas, Argentina. *In*: TANKARD, A. J., SUÁREZ SORUCO, R. & WELSINK, H. J. (eds) *Petroleum Basins of South America*. American Association of Petroleum Geologists, Memoirs, **62**, 341–357.

SPENCER, K. J. & LINDSLEY, D. H. 1981. A solution model for coexisting iron-titanium oxides. *American Mineralogist*, **66**, 1189–1201.

STEINTHORSSON, S., HELGASON, Ö., MADSEN, M. B., BENDER KOCH, C., BENTZON, M. D. & MORUP, S. 1992. Maghemite in Icelandic basalts. *Mineralogical Magazine*, **56**, 185–199, http://dx.doi.org/10.1180/minmag.1992.056.383.05

TAUXE, L. & KENT, D. V. 2004. A simplified model for the geomagnetic field and the detection of shallow bias in paleomagnetic inclinations: Was the ancient magnetic field dipolar? *In*: CHANNELL, J. E. T., KENT, D. V., LOWRIE, W. & MEERT, J. G. (eds) *Timescales of the Paleomagnetic Field*. American Geophysical Union, Geophysical Monograph Series, **145**, 101–115, http://dx.doi.org/10.1029/145GM08

THOMPSON, R. & OLDFIELD, F. 1986. *Environmental Magnetism*. Allen & Unwin, London, http://dx.doi.org/10.1007/978-94-011-8036-8

TORSVIK, T. H., MÜLLER, R. D., VAN DER VOO, R., STEINBERGER, B. & GAINA, C. 2008. Global plate motion frames: towards a unified model. *Reviews of Geophysics*, **46**, http://dx.doi.org/10.1029/20007RG000227

TORSVIK, T. H., VAN DER VOO, R. *ET AL*. 2012. Phanerozoic polar wander, palaeogeography and dynamics. *Earth-Science Reviews*, **114**, 325–368, http://dx.doi.org/10.1016/j.earscirev.2012.06.007

ULIANA, M. A., BIDDLE, K. T. & CERDAN, J. 1990. Mesozoic extension and the formation of Argentine sedimentary basins. *In*: TANKARD, A. J. & BALKWILL, H. R. (eds) *Extensional Tectonics and Stratigraphy of the North Atlantic Margins*. American Association of Petroleum Geologists, Memoirs, **46**, 599–614.

VAHLE, C. & KONTNY, A. 2005. The use of field dependence of AC susceptibility for the interpretation of magnetic mineralogy and magnetic fabrics in the HSDP-2 basalts, Hawaii. *Earth and Planetary Science Letters*, **238**, 110–129, http://dx.doi.org/10.1016/j.epsl.2005.07.010

VALENCIO, D. A. 1972. Palaeomagnetism of the lower Cretaceous Vulcanitas Cerro Colorado Formation of the Sierra de Los Cóndores Group, province of Córdoba, Argentina. *Earth and Planetary Science Letters*, **16**, 370–378, http://dx.doi.org/10.1016/0012-821X(72) 90154-9

VAN DER VOO, R. 1993. *Paleomagnetism of the Atlantic, Tethys and Iapetus Oceans*. Cambridge University Press, Cambridge.

VAN DER VOO, R., WU, F., WANG, Z., DONGWOO, S., PEACOR, D. R. & QIZHONG, L. 1993. Paleomagnetism and electronic microscopy of the Emeishan basalts, Yunnan, China. *Tectonophysics*, **221**, 367–379, http://dx.doi.org/10.1016/0040-1951(93)90168-J

VILAS, J. F. A. 1976. Paleomagnetism of the Lower Cretaceous Sierra de los Condores Group, Cordoba province, Argentina. *Geophysical Journal of the Royal Astronomical Society*, **46**, 295–305, http://dx.doi.org/10.1111/j.1365-246X.1976.tb04159.x

WARNER, R. D. & WASILEWSKI, P. 1997. Magnetic petrology of arc xenoliths from Japan and Aleutian Islands. *Journal of Geophysical Research*, **102**, 20,225–20,243, http://dx.doi.org/10.1029/97JB01517

WATKINS, N. D. & HAGGERTY, S. E. 1965. Some magnetic properties and the possible petrogenetic significance of oxidized zones in an Icelandic olivine basalt. *Nature*, **206**, 797–800, http://dx.doi.org/10.1038/206797a0

WILSON, R. L. 1966. Further correlations between the petrology and the natural magnetic polarity of basalts. *Geophysical Journal of the Royal Astronomical Society*, **10**, 413–420, http://dx.doi.org/10.1111/j.1365-246X.1966.tb03068.x